EFFECT OF WAVE FORCES ON STORM SURGE

Robert J. Weaver and Donald N. Slinn

rweaver@coastal.ufl.edu, slinn@coastal.ufl.edu

University of Florida Department of Civil and Coastal Engineering

Gainesville, FL. 32611, USA

June, 2004

Submitted for publication in *Coastal Engineering*

Abstract

The disastrous effects of hurricanes on coastal communities are well known, and there is a need to better understand the causes of storm surge to prepare for future events. To better understand the mechanisms, we examine the influence of individual factors that produce surge. The total surge depends on wind surface stress, inverted barometer effects, and wave forcing, as well as tidal stage and bathymetry in the path of the storm. We are particularly interested in the effect of wave stresses on overall surge. In the past, many models have neglected the influence of wave induced set-up. Wave stresses could be left out of numerical models for computational efficiency, when they are not a significant player. On the other hand, for conditions when wave stresses are significant, it is of interest to know if the total surge is a linear superposition of the wind and wave set-up, or if there is a more complicated relationship. Our work is a component of a real-time wind, wave, and surge forecasting system for tropical cyclones being developed under the National Oceanographic Partnership Program.

To test the rise in surface elevation, we use the Advanced Circulation Model for Coasts, Shelves, and Estuaries in two-dimensional depth-integrated mode (ADCIRC 2DDI). We conduct a suite of model studies including tests of wind stress formulation, grid resolution, and bottom friction.

To test sensitivity to coastal bathymetry, we generate three simple finite element grids on idealized coastal topographies. We use these to test three different strengths of storms. The storms range in intensity from a strong gust (10 m/s), to a medium strength tropical storm (30 m/s), to a Category 3 hurricane (56 m/s). Here, steady winds are applied on our coastal domain, and the associated wave fields are predicted using SWAN (Simulating Waves Nearshore). We examine relationships between bathymetry and set-up due to wind and waves. These tests aid us in interpreting more complicated results

from historical storm events over real bathymetry. Our results indicate that for the same wind forcing and offshore wave conditions, wave generated surge can vary for different coastal bathymetries.

The final application of our model system is a hindcast of hurricane Georges (1998). When Georges made landfall in the Biloxi, Mississippi area, it was a strong Category 2 hurricane on the Saffir-Simpson scale. We use the North West Atlantic basin for the model domain. We run the model three times, first with wind and atmospheric pressure forcing. The second time we force the model with wave radiation stresses from the predicted wave fields. The final model run combines wind and pressure fields with wave forcing. The resulting changes in surface elevation are compared with each other and with NOAA station data. We demonstrate that, in this case, to more accurately predict the surge it is necessary to include the wave forcing. Here, the wave forcing contributes approximately 25% to 33% of the total rise in water level.

Keywords: Hurricane; Storm Surge; Hindcast; Wave set-up; Tropical Cyclone; ADCIRC

1 INTRODUCTION

Tropical cyclones are low-pressure systems that form in the tropics. In the northern hemisphere the wind will rotate around the low-pressure center in a cyclonic pattern, counter-clockwise. As this low-pressure system moves over warmer waters, it can intensify. A hurricane is a strong tropical cyclone. By the time the system is classified as a hurricane, there are maximum sustained winds of 74 mph (33 m/s). The surface of the ocean under the storm will react to the pressure and wind. The threat to coastal communities from a hurricane includes high winds causing damage, as well as coastal flooding caused by the storm tide. Storm surge is the rise in water level due to hurricanes. There are three main causes of storm surge: wind set-up, wave set-up, and the inverse barometric effect of the low central pressure of the storm. The tides will also play a role in the effect of the hurricane on the coast. Storm tide is the combination of the surge with the tide. If the storm makes landfall during high tide, the effect is a higher water level than if the surge hits the shore during low tide. The wind set-up is caused by the wind blowing across the surface of the water over hundreds of square kilometers. Wave set-up is caused by the generation and then release of wave momentum (or radiation stress) in the water column as waves are formed, shoal, and then break.

Radiation stress is the flux of momentum due to waves (Longuett-Higgins and Stewart, 1964). It is the transfer of wave momentum to the water column that forces a change in the mean water level. Near the coast, wave momentum flux is balanced by a pressure gradient associated with a change in the local water depth. As wave momentum increases in the presence of non-breaking waves, the mean water level lowers. As breaking commences, the wave energy and momentum decrease, resulting in a reduction of the radiation stress carried by the waves. These stresses (force per unit area) are imparted into the water column. The rapid reduction of wave radiation

stress near the coast forces a rise in mean sea level. The discharged momentum from the waves pushes against the water column, and produces an opposing hydrostatic pressure gradient. During storm events, the resulting rise in water level can play a major role in storm surge.

According to linear theory, the effective change in water level from a steady train of linear waves approaching normal to the shore on a gently sloping bottom is about 19% of the breaking wave height (Dean and Dalrymple, 1991). This may increase or decrease as we take into account nonlinear effects, dissipative forces, and wave obliquity. The amount of wave set-up is also affected by the bottom contour of the near-shore and beach face. We examine the effect of wave radiation stress on sea surface elevation for complex forcing conditions. Our goal is to increase understanding of the role that waves play in storm surge.

1.1 Surge Model

The hydrodynamic model we use to predict the sea surface elevation is the Advanced Circulation Model for Coasts, Shelves, and Estuaries in two-dimensional depth-integrated mode (ADCIRC 2DDI) (Luettich et al., 1992). It is a finite element model that solves the conservation laws for mass and momentum through a Generalized Wave Continuity Equation in nonconservative form. We predict water level changes by driving the hydrodynamics with

- Wind stress and atmospheric pressure only
- Wave radiation stress only
- A combination of wind and wave stresses and atmospheric pressure fields.

From this series of predictions we determine the significance of including wave stresses in our model system. As a test case, we perform hindcasts of

hurricane Georges (1998) with each of the forcing options. We compare the results with water-level data for that time period, and evaluate the predictive value of including the wave forces in the model inputs.

Domain sensitivity studies have been performed using the ADCIRC model (Blain, 1997; Blain et al., 1994; Brebbia et al., 1995; Blain et al., 1998). It was found that selecting an appropriate sized domain was an important factor in the development of an accurate prediction. With a large enough domain, the key features of resonance and circulation are captured (in our case, the domain includes the Northwest Atlantic Basin with the Caribbean and the Gulf of Mexico). A benefit to such a large domain is the simplicity of the boundary conditions. The open boundaries are primarily located in the deep ocean, minimizing boundary effects on the coastal region of interest. Hagen et al. (2000, 2001) showed that sufficient grid resolution over regions of varying bathymetry is important. In these regions, a finer mesh is required to capture the evolution of the water elevation.

1.2 Air–Sea Coupling

Storm surge is dependent on wind surface stress, inverted barometer effects, tidal stage, bathymetry, and changes in wave radiation stresses. Momentum transfer at the air-sea interface produces wind-generated waves and has been studied extensively (Geernaert and Plant, 1990; Donelan et al., 1993; Donelan, 1998). The wind stress is usually approximated as $\tau = \rho C_d |U| U$ where ρ is the density of air, U is the mean wind speed taken at 10 meters above the surface, and C_d is the drag coefficient. The drag coefficient depends on sea surface roughness and atmospheric stratification, and has a magnitude on the order of 10^{-3}. There are many different recommended forms for the drag coefficient, C_d. The range of validity of the different formulas for C_d depend on wind conditions, and other factors. There has been relatively little research, however, into what formulation would best suit hurricane wind and sea conditions. It is difficult to make open ocean measurements during

hurricane conditions. Most equations produce (by extrapolating from data) an increasing drag coefficient with increasing wind speed. This formulation fits data sets at lower wind speeds. But, when the strength of the winds becomes large, the tops of the waves can be sheared and the relative wave surface roughness changes. This is analogous to a slip boundary condition. One possibility, currently being debated, is that at higher wind speeds the drag coefficient may level off as the waves are sheared off at the crests, and the net momentum imparted to the water column begins to level off. With such complicated possible scenarios, one must be aware of the sensitivity of the surge predictions to the choice of the coefficient of drag in the wind stress formulation. We pursue such sensitivity tests below and then proceed with our hindcasts using one of the standard ADCIRC formulas (Garratt, 1977) for drag coefficient (Eq. 1), with a maximum allowable drag coefficient of 0.003. The corresponding formulas for wind stress are given by Eqs. 2, 3.

$$C_d = 0.001 * (0.75 + 0.067 * U) \tag{1}$$

$$ws_x = C_d * 0.001293 * v_x(n) * U \tag{2}$$

$$ws_y = C_d * 0.001293 * v_y(n) * U \tag{3}$$

where

$U = [v_x(n)^2 + v_y(n)^2]^{\frac{1}{2}}$ — wind speed

ws_x — horizontal wind stress in x–direction

ws_y — horizontal wind stress in y–direction

$v_x(n)$ — horizontal wind velocity in x–direction

$v_y(n)$ — horizontal wind velocity in y–direction

1.3 Atmospheric Pressure

Ambient atmospheric pressures are around 1012 mb. The low-pressure center of a tropical storm causes a local rise in the sea surface. This inverted barometer effect is important when attempting to predict water levels. One

can expect around 1 cm of water rise for each millibar of pressure drop in deep water (Anthes, 1982). Though this effect may seem small, hurricane Georges had a minimum recorded central pressure of 938 mb while in the Atlantic, corresponding to a 0.75 m rise in sea surface elevation. Georges weakened by the time it made landfall on the Gulf Coast. The central pressure increased to 964 mb, corresponding to an approximate 0.5 m rise in sea level in deep water. As a storm approaches land, the height of the sea level rise associated with the inverse barometer effect can increase due to the horizontal convergence of the water. The convergence and reflection against the coastline can increase the surge level. If the barometric effect is neglected, the prediction of surge would be less than the actual rise in elevation measured at the coast.

1.4 Coastal Bathymetry

The bathymetry of the shelf and near-shore region will also play a role in the level of storm surge measured at the coastline. The magnitude of the wind blow-up is dependent on the depth and width of the continental shelf. Wind stress over a shallow wide shelf will produce a larger set-up than the same wind stress over a narrower or deeper shelf. The steady state, one-dimensional solution for wind-induced sea level rise (Dean and Dalrymple, 1991) is shown in Eq. 4.

$$\frac{\partial \eta}{\partial x} = \frac{n\tau_{zx}(\eta)}{\rho g(h+\eta)} \tag{4}$$

where

h – mean water depth

η – displacement free surface about the mean

x – cross-shore location

$n = 1 - \frac{\tau_{zx}(-h)}{\tau_{zx}(\eta)}$ and n is greater than 1

$\tau_{zx}(\eta)$ – wind surface stress in x–direction

$\tau_{zx}(-h)$ – bottom shear stress in x–direction

ρ – reference density of water

g – gravity

As seen in Eq. 4, in the deeper waters when $h \gg \eta$, the set-up goes to zero. In the depth-averaged approximation, near a coast in steady state, the horizontal velocity is zero and the bottom shear stress vanishes and $n = 1$.

We present results below of experiments concerning wave set-up on a variety of profiles. The simplest beach model is a planar beach. Many planar beach models were used to derive the approximate formulas for wave set-up (Saville, 1961; Longuett-Higgins, 1983; Stive and Wind, 1982; James, 1974; Dean and Dalrymple, 1991). For a planar beach, the mean water surface displacement from small amplitude normally incident waves is about $0.19H_b$ (Dean and Dalrymple, 1991). Komar (1998) empirically fits a more complex relationship between the slope of the foreshore and the maximum set-up elevation at the shoreline, Eq. 5, based on the Irribaren number, Eq. 6 (ratio of beach face slope to wave steepness).

$$\overline{\eta}_{max} = 0.18 g^{\frac{1}{2}} S H_{\infty}^{\frac{1}{2}} T \tag{5}$$

$$\zeta_{\infty} = \frac{S}{(\frac{H_{\infty}}{L_{\infty}})^{\frac{1}{2}}} \tag{6}$$

Where S is the slope of the bottom, H_{∞} and L_{∞} are the significant wave height and wavelength of the incident waves in deep water, and T is the wave period.

Additional studies have been performed on beaches with a concave-up Equilibrium Beach Profile, (EBP) (Dean and Dalrymple, 2002).

$$h = Ax^{\frac{2}{3}} \tag{7}$$

The results of these tests are compared to the case of a planar beach, and it was found that the set-up on a concave-up beach will mirror the bottom curvature (McDougal and Hudspeth, 1981). Smaller waves will break closer to the shoreline and the overall breaking pattern is inversely proportional to the water depth. To a first approximation, the maximum surge level will be

the same at the shoreline as for a plane beach. Farther offshore, however, the planar beach will allow for a greater increase in elevation, as the mean water level mimics the bottom contour. The EBP allows waves to propagate closer to the shoreline before breaking, imparting their momentum to the water column closer to shore than on a planar beach. The first set of tests described below were performed using the Equilibrium Beach Profile as the bathymetric contour.

Guza and Thornton (1981) developed a relation based on measurements of irregular wave set-up on beaches in Southern California, Eq. 8. The study was performed on a beach with a mild slope (0.02), where the waves break across a wide surf zone. This would be classified as a dissipative beach (Komar, 1998). The incident wave heights ranged from 0.6 m to 1.6 m.

$$\overline{\eta}_{max} = 0.17 H_{\infty} \tag{8}$$

This relation yields a result approximately 10% less than the linear solution. Our research focuses on much more powerful wave events, with time varying wave fields and complex shorelines. Our domain is the Gulf of Mexico shelf. This region has a much milder sloping beach and near-shore region than that of California. We expect more dissipation from nonlinear effects and bottom friction in our test due to this bathymetric difference.

1.5 Hurricane Simulation

For our most comprehensive numerical experiment, we perform a hindcast of hurricane Georges. Hurricane Georges made landfall in the Biloxi, Mississippi area on September 28, 1998 (Guiney, 1999). At the time of landfall the storm was rated a strong Category 2 hurricane on the Saffir-Simpson scale, with estimated maximum sustained one minute winds of 90 knots (103.6 mph, 46.3 m/s). During previous days, as the storm made its way across the Caribbean, Georges peaked as a Category 4 hurricane with estimated top wind speeds of 135 knots (155.4 mph, 69.5 m/s). The storm

caused extensive damage and loss of life. The relief effort is estimated to have cost $2.5 Billion and 602 lives were lost, predominantly in Puerto Rico, Cuba, and the Caribbean islands. We model the last 6 days of the storm, from the 25^{th} September, 1998 until the 1^{st} of October, 1998. After this time, the storm is well over land. The domain of our model predictions encompasses the North West Atlantic Basin. Our results will be compared to tidal station data at different locations on the Gulf Coast.

2 METHODOLOGY

2.1 Numerical Model

To predict the rise in surface elevation, we use the Advanced Circulation Model for Coasts, Shelves, and Estuaries in two-dimensional depth-integrated mode (ADCIRC 2DDI). ADCIRC was developed by the Army Corps of Engineers Dredging Research Program (DRP). The principal developers were J.J. Westerink and Rick Luettich (Luettich et al., 1992). One of the purposes of the research was to develop a model that could compute storm surge hydrographs and provide surface elevation data. There are four main inputs for the ADCIRC model. These include the finite element grid and bathymetry file, the numerical parameter set, the meteorological forcing and the wave forcing files. The grid is defined by node numbers and locations, element neighbors and boundary information. The input parameters include the time step, duration of the model run, coordinate system definitions, friction coefficient, horizontal eddy viscosity, output parameters, input file parameters, etc. (Luettich et al., 1992). Two other main input fields are necessary to force the model run, the meteorologic (wind stress and atmospheric pressure) and the wave stress forcing files.

The meteorological forcing file contains the wind stress and pressure data at specified time intervals. Wind stress is computed from the wind speed and direction using Eqs. 2 and 3. In order to make this conversion, we must decide on the formula to use for drag coefficient. There are numerous relationships that attempt to parameterize the drag coefficient, C_d. We tested seven different formulations, six given in Table 1 (Geernaert and Plant, 1990) and a constant value of $C_d = 0.003$.

[Table 1 about here.]

Garratt's (1977) formula represents a compilation of results calibrated for wind speeds between 4 and 21 m/sec. The ADCIRC model uses Garratt's

formula; however, the model puts a cap on the maximum value at $C_d = 0.003$. We remove this maximum requirement for the sensitivity tests. Miller (1964) proposed a maximum drag coefficient of $4.0 * 10^{-3}$, for wind speeds of 52 m/sec. The value was inferred using the ageostrophic technique. This method assumes a transfer of angular momentum in a cyclonic system which results in a cross-isobaric flow. Klapstov (1983) provides a comprehensive formulation determined from 214 records of data for wind speeds ranging from 2 to 21 m/sec. Geernaert's (1987) formula, for wind speeds of 5 to 25 m/sec, was fit to 116 data points. The Large & Pond (1981) formula is a fit to 1001 data points, for wind speeds of 10 to 26 m/sec. Smith (1980) fit 120 points for wind speeds ranging from 6 to 22 m/sec. There have been no direct measurements of drag formula for wind speeds over 26 m/sec. When Georges made landfall the estimated one minute winds were 90 knots (46.3 m/sec). Holding all other variables constant, we ran the ADCIRC model for each of the drag coefficient formulations, and determined the sensitivity of the model. Once we have decided on a satisfactory formulation, we generate the wind and pressure input file, fort.22.

The wave forcing fields specify the x and y directed wave stresses. These are also provided for every node at predetermined time intervals. We will discuss the generation of the wave fields in more detail for each test case below. Once calculated, we generate the wave forcing input file, fort.23.

The ADCIRC model output includes surface elevation and depth averaged current velocities for every node at user specified time intervals. One can also prescribe recording stations for time series of velocity and sea level at predefined time intervals for any location in the domain. The model also has the ability to perform harmonic analysis of the surface elevation.

This finite element model solves the conservation laws for mass and momentum. Conservation of mass is implemented by way of the Generalized Wave Continuity Equation (GWCE) (Luettich et al., 1992) derived from Eq. 9. The momentum equations in nonconservative form are derived from

the turbulent incompressible Navier-Stokes (Reynolds averaged) equations. First the three dimensional equations are simplified using the Boussinesq approximation and the hydrostatic pressure approximation, yielding Eqs. 10-12.

$$\frac{\partial u}{\partial x}+\frac{\partial v}{\partial y}+\frac{\partial w}{\partial z}=0 \tag{9}$$

$$\frac{\partial u}{\partial t}+u\frac{\partial u}{\partial x}+v\frac{\partial u}{\partial y}+w\frac{\partial u}{\partial z}-fv=-\frac{\partial}{\partial x}\big[\frac{p}{\rho_0}-\Gamma\big]+\frac{1}{\rho_0}\big[\frac{\partial \tau_{xx}}{\partial x}+\frac{\partial \tau_{yx}}{\partial y}+\frac{\partial \tau_{zx}}{\partial z}\big] \tag{10}$$

$$\frac{\partial v}{\partial t}+u\frac{\partial v}{\partial x}+v\frac{\partial v}{\partial y}+w\frac{\partial v}{\partial z}+fu=-\frac{\partial}{\partial y}\big[\frac{p}{\rho_0}-\Gamma\big]+\frac{1}{\rho_0}\big[\frac{\partial \tau_{xy}}{\partial x}+\frac{\partial \tau_{yy}}{\partial y}+\frac{\partial \tau_{zy}}{\partial z}\big] \tag{11}$$

$$\frac{\partial p}{\partial z}=-\rho g \tag{12}$$

where

$f = 2\Omega sin\phi =$ Coriolis parameter

$g =$ acceleration due to gravity

$\Gamma =$ tide generating parameter

$\nu =$ molecular viscosity

$p(x, y, z, t) =$ time-averaged pressure

$\rho(x, y, z, t) =$ density of water

$\rho_0 =$ reference density of water

$t =$ time

$T =$ integration time scale for separating turbulent and time-averaged quantities

$\tau_{xx}(x, y, z, t) = \nu[2\frac{\partial u}{\partial x}] - \frac{1}{T}\int_0^T u'u'dt$ – combined viscous and turbulent Reynolds stress

$\tau_{yx}(x, y, z, t) = \nu[\frac{\partial u}{\partial y} + \frac{\partial v}{\partial x}] - \frac{1}{T}\int_0^T u'v'dt$ – combined viscous and turbulent Reynolds stress

$\tau_{zx}(x, y, z, t) = \nu[\frac{\partial u}{\partial z} + \frac{\partial w}{\partial x}] - \frac{1}{T}\int_0^T u'w'dt$ – combined viscous and turbulent Reynolds stress

$\tau_{xy}(x, y, z, t) = \nu[\frac{\partial v}{\partial x} + \frac{\partial u}{\partial y}] - \frac{1}{T}\int_0^T v'u'dt$ – combined viscous and turbulent Reynolds stress

$\tau_{yy}(x, y, z, t) = \nu[2\frac{\partial v}{\partial y}] - \frac{1}{T}\int_0^T v'v'dt$ – combined viscous and turbulent Reynolds stress

$\tau_{zy}(x,y,z,t) = \nu[\frac{\partial v}{\partial z} + \frac{\partial w}{\partial y}] - \frac{1}{T}\int_0^T v'w'dt$ – combined viscous and turbulent Reynolds stress

ϕ = degrees latitude

$u(x,y,z,t), v(x,y,z,t), w(x,y,z,t)$ = time-averaged velocities in the x, y and z directions

$u'(x,y,z,t), v'(x,y,z,t), w'(x,y,z,t)$ = departures of the instantaneous turbulent velocities from the time-averaged velocities

x, y = horizontal coordinate direction

z = vertical coordinate direction

Ω = angular speed of the Earth (7.29212x10^{-5} rad/s)

After eliminating pressure as a dependent variable using 12 and defining the top and bottom boundary conditions, Eqs. 9, 10 and 11 are vertically integrated to yield two-dimensional equations for free surface displacement and depth-averaged velocity. The depth-integrated form of the continuity equation is given by Eq. 13. The vertically integrated momentum conservation equations are given by Eq. 14 and 15.

$$\frac{\partial \zeta}{\partial t} + \frac{\partial UH}{\partial x} + \frac{\partial VH}{\partial y} = 0 \tag{13}$$

$$\frac{\partial U}{\partial t}+U\frac{\partial U}{\partial x}+V\frac{\partial U}{\partial y}-fV = -\frac{\partial}{\partial x}[\frac{p_s}{\rho_0}+g(\zeta-\alpha\eta)]+\frac{1}{H}[M_x+D_x+\frac{\tau_{sx}}{\rho_0}-\frac{\tau_{bx}}{\rho_0}] \tag{14}$$

$$\frac{\partial V}{\partial t}+U\frac{\partial V}{\partial x}+V\frac{\partial V}{\partial y}+fU = -\frac{\partial}{\partial y}[\frac{p_s}{\rho_0}+g(\zeta-\alpha\eta)]+\frac{1}{H}[M_y+D_y+\frac{\tau_{sy}}{\rho_0}-\frac{\tau_{by}}{\rho_0}] \tag{15}$$

where

α = effective Earth elasticity factor ($\alpha = 0.69$)

$D_x \equiv -\frac{\partial D_{uu}}{\partial x} - \frac{\partial D_{uv}}{\partial y}$ — momentum dispersion

$D_y \equiv -\frac{\partial D_{uv}}{\partial x} - \frac{\partial D_{vv}}{\partial y}$ — momentum dispersion

$D_{uu} \equiv \int_{-h}^{\zeta} \hat{u}\hat{u}dz, D_{uu} \equiv \int_{-h}^{\zeta} \hat{v}\hat{u}dz, D_{uu} \equiv \int_{-h}^{\zeta} \hat{v}\hat{v}dz$

$\eta(x,y,z)$ — Newtonian equilibrium tidal potential

$M_x = \frac{\partial}{\partial x}\int_{-h}^{\zeta}\frac{\tau_{xx}}{\rho_0}dz + \frac{\partial}{\partial y}\int_{-h}^{\zeta}\frac{\tau_{yx}}{\rho_0}dz$ — depth-integrated, horizontal momentum diffusion

$M_y = \frac{\partial}{\partial x}\int_{-h}^{\zeta}\frac{\tau_{xy}}{\rho_0}dz + \frac{\partial}{\partial y}\int_{-h}^{\zeta}\frac{\tau_{yy}}{\rho_0}dz$ — depth-integrated, horizontal momentum diffusion

$U(x,y,t) \equiv \frac{1}{H}\int_{-h}^{\zeta} u dz$ — depth-averaged horizontal velocity

$V(x,y,t) \equiv \frac{1}{H}\int_{-h}^{\zeta} v dz$ — depth-averaged horizontal velocity

$\hat{u}(x,y,z,t) \equiv u - U$ — departure of horizontal velocity from depth-averaged velocity

$\hat{v}(x,y,z,t) \equiv v - V$ — departure of horizontal velocity from depth-averaged velocity

$H(x,y,t) \equiv \zeta + h$ — total water depth to free surface

ζ — free surface

$h(x,y)$ — bathymetric depth relative to geoid

τ_{sx}, τ_{sy} — applied free surface stresses

τ_{bx}, τ_{by} — applied bottom stresses

The bottom stresses are replaced by a quadratic friction term. The equations are differentiated and combined to get the GWCE. DSRP-92-6, Report 1: Theory and Methodology (Luettich et al., 1992) gives a complete description.

2.2 Bathymetric Tests

The first set of tests we perform are a series of experiments examining set-up over idealized bathymetric conditions for different wind and wave conditions. Our purpose is to determine the model response to separate and combined influences of variations in wind speed, wave height, and water depth.

2.2.1 Domain

We generate wind and wave fields over three bathymetries. Contours are created, Figure 1, using the equilibrium beach profile method (Dean and

Dalrymple, 2002):

$$h = Ax^{\frac{2}{3}} \qquad A = 0.2, 0.1, 0.05 \tag{16}$$

[Figure 1 about here.]

Where A is a parameter based on the average grain size of the near-shore sediment, x is the cross-shore distance and h is water depth. We define the average near-shore slope as the slope from the shore, $x = 0$, to the water depth at $x = 1$ km. The beach profiles have average near-shore slopes of 0.017, 0.0091 and 0.004, from steepest to mildest. Farther offshore, in the region 2 km to 20 km, the average slopes are 0.0065, 0.0028 and 0.0017, respectively. The profile is uniform in the alongshore. We generate a finite element grid, Figure 2, for the model domains using ACE/gredit (Turner and Baptista, 1999). Resolution at the shoreline is on the order of 20 meters, and decreases as the depth increases.

[Figure 2 about here.]

2.2.2 Forcings

Three different strength shore normal winds are chosen. The weakest wind forcing is a 10 m/s wind that corresponds to a strong gust. The intermediate case is a 30 m/s wind, corresponding to a medium strength tropical storm. The strongest wind used corresponds to a Category 3 hurricane on the Saffir-Simpson scale, with a 56 m/s wind speed. The associated wave forces were generated using SWAN (Simulating Waves Near-shore) (Holthuijsen, 2000). The offshore wave heights specified are 1.0 m, 5.0 m, and 7.0 m, corresponding to the wind speeds of 10, 30 and 56 m/s respectively (Table 2).

[Table 2 about here.]

These offshore wave heights were selected after a series of iterations with SWAN, keeping the wind speed constant. Our applied winds are uniform

in time and space. The domain SWAN uses to compute the wave fields is 20 km cross-shore and 50 km along-shore. We make sure that the along-shore direction is large enough that the center line of the domain will be unaffected by boundary effects. SWAN uses a Cartesian computational grid with 5 m spacing. The wave fields generated in SWAN are based on a JONSWAP distribution with directional spreading of 5 degrees. Bottom friction is turned on, as is white-capping. The SET-UP function is also turned on. SWAN outputs the momentum transfer from the wave field to the depth averaged currents by integrating the radiation stresses over the wave direction and frequency spectrum. The x and y components of the momentum transfer are

$$F_x = \frac{1}{\rho}[-\frac{\partial S_{xx}}{\partial x} - \frac{\partial S_{xy}}{\partial y}] \tag{17}$$

$$F_y = \frac{1}{\rho}[-\frac{\partial S_{yy}}{\partial y} - \frac{\partial S_{yx}}{\partial x}] \tag{18}$$

where

$S_{xx} = \rho g \int \left[ncos^2\theta + n - \frac{1}{2}\right] Ed\alpha d\theta$

$S_{xy} = S_{yx} = \rho g \int \left[nsin\theta cos\theta\right] Ed\alpha d\theta$

$S_{yy} = \rho g \int \left[nsin^2\theta + n - \frac{1}{2}\right] Ed\alpha d\theta$

$n = \frac{C_g}{C}$

The wave heights and forcings output by SWAN are shown in Figure 3 and Figure 4, respectively, for the three bathymetric contours and three specified wind fields.

[Figure 3 about here.]

[Figure 4 about here.]

The wind speed is converted into a wind stress for ADCIRC as described previously and then interpolated to the finite element grid, Figure 2. Using ADCIRC, we test the change in sea level for three scenarios

- atmosphere forcing only
- wave forcing only
- combined wind and wave forcing.

2.2.3 Implementation

The time step for ADCIRC is determined by the Courant number and is set such that $C_{\#} < 1.5$. The Courant number is given as

$$C_{\#} = \frac{(gh)^{\frac{1}{2}}\Delta t}{\Delta x} \tag{19}$$

On the finely resolved grid, a time step of 0.10 sec is necessary to ensure reliable, stable results. With such a small time step, the total run length needs to be as short as possible, but long enough for the system to reach equilibrium. We use time weighting factors for the free surface terms in the GWCE of 0.35, 0.30 and 0.35. The free surface terms at the K^{th} time level are weighted by $g * (0.35 + 0.30)$. These terms at the $K - 1$ time level are weighted by $g * 0.35$. These factors are chosen such that the sum is 1.0. The initial conditions are $u = v = \eta = 0$. In order to damp out the wave created by the initial overshoot of the equilibrium position, the model is ramped up by gradually introducing the forcing over 6 hours and the bottom friction is increased to 0.06. This is acceptable because we are interested in obtaining a steady state solution in which the depth averaged currents and associated bottom stresses are zero. In SWAN, for the wave fields, we used the more realistic default bottom friction, the semi-empirical formula derived from the JONSWAP results (Holthuijsen, 2000).

The factor that weights the wave and primitive continuity contributions to the GWCE is set to match the value of the friction coefficient as recommended in the ADCIRC manual, $\tau_o = 0.06$. Without these steps an overshoot wave will seiche through the basin, potentially introducing a numerical instability or requiring a smaller time step and take much longer to achieve steady

state conditions. Taking the ramp-up time into consideration, we obtain a steady state set-up by running the model for a period of 1 day. For this grid resolution, a model run takes approximately 2 days of CPU time on a 3.0 GHz Pentium processor. After inspecting the output, we notice that the system equilibrates after approximately 18 hours.

2.3 Hurricane Georges Hindcast

We conducted a hindcast of a historical storm event. The landfall of hurricane Georges on the Mississippi coast was chosen as the subject storm. In order to accomplish this we needed to decide on the proper model domain and forcings to be used. We also obtained historical data to compare to our surge predictions from the NOAA National Ocean Service Center for Operational Oceanographic Products and Services, (NOAA NOS CO-OPS) web site.

2.3.1 Domain

It is important to ensure that the domain is large enough to capture the true resonant characteristics of a basin (Blain et al., 1998). We also want to formulate our modeling system to accommodate the majority of tropical cyclones so we can have a general use domain for future model forecasts. The model domain is the North West Atlantic Basin, including the Caribbean Sea and the Gulf of Mexico, Figure 5.

[Figure 5 about here.]

This grid was provided by Rick Leuttich. With such a large domain, we have the ability to model any storm that enters the western Atlantic, not just the Gulf of Mexico. In addition, the only open boundary is at the easternmost wall. This is far enough from the coastlines of interest that boundary effects will be minimized. In the case of hurricane Georges, our simulation starts

as the storm enters the Gulf of Mexico between Florida and Cuba, and lasts until after landfall.

The region of landfall is shown in Figure 6. From this perspective we are able to see the relatively high resolution in the coastal region.

[Figure 6 about here.]

2.3.2 Forcing

Our forcings for hurricane Georges are provided by the NOPP partners. The wind and pressure inputs are a product of satellite, aircraft flight level, and buoy data from the National Hurricane Center, assimilated by Ocean-Weather Inc. (Cardone and Cox). The data are given over the whole domain, 5N–53N and 99W–50W, in 30 minute intervals, on a 0.20 degree Cartesian grid. The wind and pressure fields are then interpolated onto the finite element grid, Figure 5. The wind speed is converted into a wind stress as described previously. The wind stress and pressure are then written out to the meteorological forcing file, fort.22, to be read by ADCIRC.

Wave fields were generated by Robert Jensen at the US Army Corps of Engineers, Engineer Research and Development Center (ERDC). The assimilated wind and pressure data are used to force WAM-3G (Wave Action Model, Third Generation) (Komen et al., 1996). Wave fields are calculated at two resolutions over the portion of the domain shown in Figure 7

[Figure 7 about here.]

The coarser resolution data set, 0.2 degree, is given over a basin domain consisting of the Gulf of Mexico, portions of the Caribbean and Northwest Atlantic. A finer resolution grid, 0.1 degree, is provided for the region of interest near landfall along the Gulf Coast, including the coastal regions of Louisiana, Mississippi, Alabama, and Florida. The domains for the inputs are given in Table 3. The finer resolution wave field is the wave region. The

resolution for the wave region is 0.1 degree. The resolution for the wave basin and wind and pressure fields is 0.2 degree.

[Table 3 about here.]

Wave data is provided as wave height, peak period, and mean direction on the Cartesian grid. The gradients of the radiation stresses are calculated using 2^{nd} order central differences everywhere except at the boundaries where a first order forward difference is implemented. The forcing is then calculated from the gradients using Eqs. 20,21.

$$F_x = -\frac{1}{\rho}\left[\frac{\partial S_{xx}}{\partial x} + \frac{\partial S_{yx}}{\partial y}\right] \tag{20}$$

$$F_y = -\frac{1}{\rho}\left[\frac{\partial S_{yy}}{\partial y} + \frac{\partial S_{xy}}{\partial x}\right] \tag{21}$$

where

$S_{xx} = \frac{E}{2}(2ncos^2\theta + (2n-1))$

$S_{xy} = S_{yx} = Encos\theta sin\theta$

$S_{yy} = \frac{E}{2}(2nsin^2\theta + (2n-1))$

$n = \frac{C_g}{C}$

The momentum forcing is then interpolated to the finite element grid, Figure 5. The finer domain data is nested in the coarser set during the interpolation process. This data set is output to the wave forcing file, fort.23, to be read by the ADCIRC model.

2.3.3 Implementation

Due to the larger grid resolution used for the hurricane predictions, the Courant number stability does not play such a restrictive role as in the idealized beach experiments. For the hurricane Georges hindcast, we use a time step of 30.0 seconds. Our friction coefficient is set to a more realistic value of 0.006, as is the GWCE weighting factor, $\tau_o = 0.006$. The time weighting factors for the GWCE are 0.35, 0.30 and 0.35. We run the model for 6

days, ramping the forcings up over 0.5 day. The input data is provided at 30 minute intervals, and the initial conditions are $u = v = \eta = 0$.

This defines our problem and our method for developing a solution. We run the models for the two geometries and each input parameter that we have set. We report on the results of our numerical experiments below.

3 RESULTS

3.1 Wind Stress

The first test we perform using the Advanced Circulation Model for Coasts, Shelves, and Estuaries (ADCIRC) is a test of the drag coefficient and wind stress formulation. We test seven drag coefficient formulations, the six given in Table 1, and the constant value, $C_d = 0.003$. Figure 8 shows how each of the drag coefficient formulations responds to wind speed.

[Figure 8 about here.]

The Miller coefficient, $4.0{*}10^{-3}$, was developed for wind speeds over 50 m/sec. The plot of $3.0 * 10^{-3}$ represents the maximum value for C_d that is usually allowed in ADCIRC. Other formulas are fitted to data sets for which wind speeds vary from 2 to 26 m/sec. Garratt's formula fits the middle of the spread of the remaining formulas.

The resulting wind stress magnitudes are plotted in Figure 9.

[Figure 9 about here.]

Notice that at high wind speeds each of the formulas keeps increasing, passing the $C_d = 0.003$ cutoff. Geernaert's formula increases more rapidly than the others, reaching the cutoff value sooner. Garratt's, the standard formulation in ADCIRC, and Klapstov's formulas produce results that lie in the middle of the other plots. At lower wind speeds all the formulations, except the two constants, behave similarly.

The wind stress values are calculated for hurricane Georges. These stress values are used as inputs to force the ADCIRC model. The results of maximum set-up and set-down during the storm from the seven tests are shown in Figure 10.

[Figure 10 about here.]

Early in the simulation, as the storm enters the domain and makes its way across deeper waters, all but the two constant formulations are in close agreement. We would expect Miller's approximation to be greater than the others throughout the domain. During the time associated with the simulation, hurricane Georges was a Category 2 storm with winds less than 50 m/sec. We also see that the surge level associated with the cutoff value for C_d is greater than the results associated with the other formulations. The surge driven by Geernaert's formula comes close to that forced by the cutoff value, but only for a short period of time. The water elevation predicted using the wind stresses generated by Garratt's simple formula and Klapstov's more complicated formula, lie in the middle of the other predictions. Our purpose of conducting these tests was to quantify the sensitivity of the surge response to the wind stress parameterization, and to estimate error bars associated with this uncertainty. Without further insight into the optimal drag coefficient response to high winds, we accept the Garratt formulation; as it is simple and seems to capture the middle of the road solution. We recognize that the resulting surge prediction can vary as much as ± 0.5 meter depending on the choice of drag coefficient formulation. Similar sensitivity tests were conducted for the coefficient of bottom friction, and a moderate value of 0.006 was selected.

3.2 Bathymetric Sensitivity

Now we examine the results of the bathymetric sensitivity tests with varied forcings.

[Figure 11 about here.]

The wave heights and forcing components output by SWAN are shown in Figure 3 and Figure 4, respectively, for each bathymetric profile and forcing pair. From these results we calculate the integral $\overline{F} = \int_0^{offshore} F_x dx$, for $F_x > 0$. The magnitude of $\overline{F}$ will give us an idea of what to expect for

the surge. Figure 11 shows the magnitude of the integrals for each forcing level over each profile. We see a trend of decreased $\overline{F}$ as the profiles get shallower. This difference in $\overline{F}$ becomes more pronounced as the forcing level increases. The larger waves associated with the stronger forcing, will have a greater interaction with the bottom boundary. Dissipative effects of bottom friction will play a larger role for these cases. Across the shallower domains, the waves will break farther from shore. The wind stress imparted on the water column prior to breaking will therefore be smaller than over a steeper profile. It follows that the wave height at breaking will be smaller, as shown in Figure 3. Breaking farther offshore also allows more dissipation in a wider surf zone than the steep domain.

Having obtained our wave forcing components with SWAN, we use ADCIRC to test the change in sea level for each set of forcings : wind, wave, wind and wave. The results are summarized in Table 4 and Figure 12.

[Table 4 about here.]

[Figure 12 about here.]

The level of wind set-up varied depending on the steepness of the bathymetric profile. For each level of input forcing, the wind set-up was greatest over the shallow bathymetry and the set-up decreased as the profile became steeper (Figure 12). This is in agreement with the governing equation, Eq. 4, for the steady state solution for wind set-up.

The equilibrium state for the water surface elevation, calculated for the different wave stresses alone, also varied over the different bathymetric profiles. The steady state solution for wave set-up over a mildly sloping bottom is given by Eq. 22 (Dean and Dalrymple, 1991).

$$\frac{d\overline{\eta}}{dx} = -\frac{1}{\rho g(h+\overline{\eta})}\frac{dS_{xx}}{dx} \tag{22}$$

where

$\overline{\eta}$ — mean surface displacement

After some simplifications it can be shown that at the shore, the equation for the surface displacement can be approximated by Equation 23.

$$\overline{\eta}(0) = \overline{\eta_b} + \frac{\frac{3\kappa^2}{8}}{1 + \frac{3\kappa^2}{8}} h_b \tag{23}$$

where

$\overline{\eta_b}$ — mean surface displacement at breaking

h_b — depth at breaking

κ — breaking constant

Thus, by this approximation, the wave-induced set-up of identical wave fields at the shore is independent of the profile. The approximation also assumes that the breaking constant (and breaker type) is the same for each profile and each forcing strength, for our tests $\kappa = 0.73$. We have shown above, however, that our results predict a decrease in wave set-up for the same offshore wave forcing strength (wave stresses predicted by SWAN) as the profiles become more shallow. In part this can be attributed to different steady wave fields developing over different bathymetries for the same wind field conditions. To better understand the results we compare the ADCIRC results with the analytic solution, Eq. 22. This comparison, presented in Figure 13, shows that the model results are in close agreement with the analytic steady state solution for the mild and strong forcing cases.

[Figure 13 about here.]

We see that the cases of the weak wave forcing over the mild and steep bathymetry are not sufficiently resolved on the 20 meter ADCIRC grid to capture the full set-up at the shoreline. Though the finite element model and theory agree outside of the breaking region, the model output under predicts the surge level. Grid spacing at the shoreline for the circulation model is too

coarse to reasonably resolve the spatial gradients of breaking for the small amplitude wave cases. For more intense forcing components, the 20 meter spacing adequately resolves the system. In these cases the ADCIRC results agree with the results predicted by Eq. 22 when calculated with the SWAN output. It is the variation in wave forcing fields calculated by SWAN that produces different wave-induced set-up for similar wind forcing conditions. This variation is caused by altered breaking wave conditions that develop due to the differences in the lengths of the region of the wind fetch prior to breaking.

The predicted variation in the level of wave set-up over the different bathymetries is dependent on the strength of the forcing. Total dissipative effects are increased for increased wave heights. Large waves feel the bottom more strongly than smaller waves, and the effect of bottom friction in SWAN plays a greater role in the case of larger wave heights. These effects are reflected in the output from SWAN and translated to the results of the circulation model.

Figure 12 shows that the surge from the combined forcing is smallest over the mild profile. Peak wind set-up occurs over the shallow profile, and the peak wave set-up occurs over the steep profile. The level of wind set-up is fetch limited. Our domain is only 20 km in the cross-shore. We would expect that over a larger cross-shore domain, the winds would begin to dominate the storm surge.

In summary, the results show that the importance of the waves increases as the profile becomes steeper. Set-up due to waves does vary over the different profiles, and the steeper profile allows for a greater wave-induced set-up than the shallower profile. In addition, the wind has less of an effect on the steeper profiles, and thus the waves dominate the set-up. Winds play a larger role when the domain has a wide shallow shelf. On the shallow profile, the wind induces the majority of the set-up. In both cases, our test results indicate that waves make a significant contribution to the resulting

surge levels. These results, however, are specific to the present, fetch limited, idealized domains. The next step is to examine what happens when we use realistic temporally and spatially dependent wind fields, include a variable pressure field, compute the associated wave fields, and run the models over a real domain with complex coastal bathymetry.

3.3 Hurricane Georges

We perform a hindcast of hurricane Georges. Elevation output from ADCIRC is converted into a time series of contour plots showing the water level as hurricane Georges makes its way from the Straits of Florida to the Gulf Coast. A series of these plots is shown in Figure 14. Time is measured from t=0 on September 25 at 00:00 hour. The eye of the storm enters the Gulf, t = 30.00 h, and moves northwest. The model captures the inverted barometer effect under the eye, and the set-up and blow-down as the eye passes and winds shift direction. Set-up is produced on the windward side of barrier islands and in the bays.

[Figure 14 about here.]

We compare contour plots at the same time from three different forcing predictions. The difference between wind and pressure only, wave only, and combined wind, pressure and wave forced simulations are evident in Figure 15.

[Figure 15 about here.]

The difference in surface elevation in the back of bays is greatest. The hurricane winds are blowing in a cyclonic (counter-clockwise) pattern. Depending on the orientation of the shore to wind direction, we observe either set-up or set-down at the land boundary. In the case of waves only, the model predicts an initial set-down just offshore of the barrier islands. The water level then rises closer to the land boundaries. For the combined forcing prediction the

effects of wave set-up reduce the net set-down at the land boundary caused by the wind and pressure only. Offshore, in the region of wave set-down, the blow-up from the wind is reduced. The contour plots give us a general indication of the spatial distribution of the water surface. For a more quantitative representation, we plot the time series of the water elevation at different locations.

A time series of the maximum surge predicted over the whole domain is given by Figure 16.

[Figure 16 about here.]

The combined, wind, pressure, and wave forced prediction is greater than the predictions for separate forcings for nearly the whole time series. There is a point, about 25 hours into the prediction, when the results forced only by the waves exceed the combined results. From approximately t=25 hours to t=35 hours the maximum elevation from combined forcing decreases rapidly, and the wave forced results can be the largest of the three predictions. This surge is not associated with the hurricane making landfall, but with waves reaching the shore while the eye is still in open water. Wind and waves can work with each other forcing in the same direction, and produce a large set-up. The two can also oppose each other and reduce the maximum surge, when the wind is blowing down the area where the waves are setting-up, as is seen in these time series. These scenarios illustrate the complex nature of the system. We also note that for the combined forcing prediction, the maximum surge in the domain is always greater than or equal to the wind only prediction. The addition of wave forcing to the model produces an increase in the maximum water elevation, over the whole domain, on the order of 0.4 meter over the meteorologic forcing alone (during the peak hours).

In the analysis above we compared the maximum surges produced in the model domain. These maximum elevations, however, do not necessarily correspond to the same locations. At specific locations we may observe a

greater difference between the meteorological and combined forcing predictions. Therefore, it is of interest to examine the behavior of the sea surface at specific locations. We choose locations where historical water level data is available and associate these with nearest nodes on our grid. In addition to selecting station locations, we also retrieve data at three prescribed locations: Mobile Bay, AL, Perdido Bay, FL, and Lake Borgne, LA.

[Figure 17 about here.]

[Table 5 about here.]

The maximum elevation over the entire duration of the simulation for each forcing combination is plotted, for selected locations given by Table 5, in Figure 17. Also plotted is the maximum difference in water level between the experiment with meteorological forcing and that with combined forcing achieved at any time during the simulation. From this plot we can infer that the difference between the total water elevation and the wind forced set-up comes from the addition of wave forcing. The maximum difference is less than the surge predicted by the wave only forced run in all cases shown. This indicates that the effect of combining the forcings in the model run in not simply a linear superposition of the separate surge levels.

So far we have looked at spatial maxima and temporal maxima. These have given us an indication of the maximum observed effects of adding wave forcing to wind and pressure and how the sea surface responds. Next we look at the time history of water level at individual locations. The behavior of the sea surface is particularly interesting at the two following locations even though there was no station data available there.

[Figure 18 about here.]

We start with the location at Perdido Bay, FL, Figure 18, since it had the greatest level of wave set-up. The maximum surge due to the waves has a slightly greater magnitude than the surge from the meteorologic forcing. The

wind forced case achieves its maxima about 6 hours after the wave forced simulation, consistent with the observation that storm waves often reach the shore before the storm's strongest winds. The combined forcing run is less than the linear combination of the wind and waves separately, yet is approximately 1 meter higher than the wind and pressure forced prediction.

A second noteworthy location is Lake Borgne, LA, shown in Figure 19.

[Figure 19 about here.]

At this location we can see the dramatic effect of the eye passing. The drop in water elevation takes place over a 30 hour period, approximately t = 80 h to t = 110 h. During this time the water level goes from being pushed up about 2.4 meters, to being blown down about 2.4 meters. The node at that location is considered 'dry' (Elevation = 0), and oscillates with wetting and drying between approximately t = 135 h and t = 145 h. The peak surge calculated with combined forcing is about 40 centimeters greater than that computed using just the meteorologic forcing.

The output from the numerical model is compared to historical data obtained from the NOAA National Oceanographic Data Center, (NODC). We focus on two stations where the surge is greatest. In order to provide the best estimate, we add in the astronomical tides. Our NOPP partner, Scott Hagen, at the University of Central Florida has provided us with a tidal prediction at each of the locations of interest, using ADCIRC on a finer resolution grid over a longer duration simulation. These modeled tides match the observed phase at the stations. With the tides added, we have a comprehensive prediction of the water level.

We also rectify the definition of mean sea level between our plots and the station data. ADCIRC defines the mean water level as zero. The station data is referenced to the mean lower low water convention, MLLW. From the station data, we estimate the predicted mean water level for the time of our simulation as +0.3 meter. When we add this offset to our prediction the results can be compared.

[Figure 20 about here.]

Figure 20 shows that we improve our prediction of the peak elevations at Pensacola, Florida by 60% with the addition of wave forcing to the wind stress and atmospheric pressure. On either side of the peak, the model under-predicts the water elevations. The prediction is off by as much as 0.44 meter, with the greatest differences occurring 10 to 20 hours on either side of the peak. These coincide with the low tide cycles. The mean difference between the station data and the combined forcing prediction is 0.11 meter. This is 50% less than the mean difference between the station data and the meteorological forcing (0.20 meter). We quantify the error in our prediction by computing the mean square error, (MSE), and the root mean square error, (RMSE), normalized by the maximum elevation recorded by the station using Eqs. 24, and 25.

$$\mathrm{MSE}(\mathrm{WL1},\mathrm{WL2}) = \frac{1}{N}\sum_{i=1}^{N}(\mathrm{WL1}(i)-\mathrm{WL2}(i))^2 \tag{24}$$

$$\mathrm{RMSE}(\mathrm{WL1},\mathrm{WL2}) = \frac{\left[\frac{1}{N}\sum_{i=1}^{N}(\mathrm{WL1}(i)-\mathrm{WL2}(i))^2\right]^{\frac{1}{2}}}{\mathrm{MAX}(\mathrm{WL1})} \tag{25}$$

where

N – number of data records

WL1 – station water level record

WL2 – model prediction

The MSE for the combined forcing is 0.03 m^2. For the wind and pressure prediction the MSE is 0.09 m^2. In this case, the normalized RMSE improves from 20% to 10% by including the waves in the model prediction, a 50% reduction in error.

At the Waveland location, we estimate a mean water level of +0.35 meters. Using this mean water level we translate the model results. Figure 21 shows good agreement before and during the storm.

[Figure 21 about here.]

With only the meteorologic forcing, the model under-predicts the water level at t=79 hours by approximately 0.4 meter in Waveland, MS (Figure 21). When the waves are added the prediction achieves the peak water level at t=79 hours to within 0.005 meter. The peak water elevation for our predictions, however, does not occur at t=79 hours. The predicted peak water level of 1.98 meters, for the combined forcing case, occurs at t=80 hours. The difference between the station data peak and the combined forcing peak is 0.05 meter. The mean difference between the prediction and the station water level is 0.1 meter. We compute the MSE to be 0.08 m^2 with the waves added. This improved from the MSE of the wind and pressure forced run of 0.11 m^2. The normalized RMSE, computed with Eq. 25, for the combined forcing case is improved from 17% to 14% by adding the waves. A major source for error at this location occurs after the storm has passed, t $>$ 120 h. Our model over-predicts the amount of set-down by as much as 0.75 meter. The second largest source for error is just before the peak of the surge, when the tidal cycle is low.

We perform the same error analysis for the time period of t = 40 h to t = 110 h. During this period, we find that the MSE improves from 0.15 m^2 to 0.06 m^2 with the addition of the wave forcing. The normalized RMSE improves from 20% to 13%, almost cut in half, by including the waves.

[Figure 22 about here.]

Above, our bathymetric sensitivity tests have shown that grid resolution can play a role. In order to be sure that we have resolved the system adequately, we refine the finite element grid, Figure 5, by splitting each element into four. In doing so we increase the number of nodes from 31435 to 121296. The surface response from combined forcing and wave only forcing is compared at the Pensacola location and the Waveland location. We also compare the maximum surface elevation response to the two forcing cases. These

comparisons are shown in Figure 22. We can see from the plot that the two are in close agreement; however, the computational time for the higher resolution grid is on the order of 5 times longer. We determine that our system is adequately resolved and the model runs in an efficient time frame with the current grid.

The results show that the effect of including waves in the model forcing depends on the location. The waves can have a large effect as in the case of Perdido Bay, FL. In the comparisons of our results with historical data, we find that by adding the wave forcing we are better able to predict the peak water level. Alternately, at some locations the addition of wave forcing may not provide a significant improvement to the predictive power of the model. Predictions made by forcing the model with only the meteorologic constituents would suffice at those locations; however, we cannot know which locations those are without the combined forcing prediction results. The implications of the results are discussed Chapter 4.

4 CONCLUSIONS

The ADCIRC tests demonstrate that the addition of wave forces can result in a 30% to 50% increase in sea surface elevation. The results are sensitive to the station location with respect to the storm, coastal features such as bays and islands and grid resolution in the near-shore region. The model captures the set-up and set-down for idealized bathymetries in close agreement with analytical solutions for steady state conditions. Model sensitivity to the drag coefficient, C_d, formulation has been shown to effect the results by as much as 0.5 meter. We selected the Garratt (1977) formula because it produced results that were close to the mean of the various formulations. However, further research toward the parameterizations of air-sea interaction at high winds is needed.

4.1 Bathymetry

We observe from the bathymetric tests that the depth profiles have an effect on the wave-induced set-up. The wave field is sufficiently altered by dissipative forces to effect a change in the on-shore momentum transfer. Wind duration and fetch will also effect the breaking wave height. Wind has a chance to impart more of its energy into the water column before the waves break over the steeper profile, resulting in a larger breaking wave height. We conducted 27 tests for the nine combinations of wind speed and bathymetry with wind, wave and combined forcing. The output from the wave model, SWAN, was converted to input for the circulation model, ADCIRC. We also used the SWAN output in computing the steady state analytical solution. Our ADCIRC domain grid was too coarse to fully resolve near-shore wave breaking in the case of the one meter waves; however, we were able to resolve the stronger wave forcing over each of the bathymetries. Upon comparing the ADCIRC results with the analytical solution, we find that with adequate resolution the two are in close agreement. Grid resolution at the shoreline

is important. In the cases where the breaking is resolved, the model only slightly under-predicts the analytical solution. The fact that we obtain such close agreement with theory reinforces our confidence in the output of the circulation model. Our results indicate that a reduction in the wave-induced set-up occurs when the waves propagate over a wide shallow shelf. As the profile steepens, the wave set-up will increase.

Wind induced set-up is also a function of the bathymetry. Shallow profiles allow for a larger set-up for the same wind strength compared to steeper profiles. The level of surge from winds is also influenced by the fetch. In our case we have a relatively short fetch, thus reducing the level of wind set-up. Were we to increase the cross-shore domain of our simulation, we would expect to see the wind set-up increase and dominate the system.

For the strongest forcing runs, the combined wind and wave forcing runs for our domain are largest over the steep domain, where the waves dominate. The winds dominate over the shallow profile, and there we have the second highest surge. Over the mild domain, both contribute approximately equally and we see the smallest total set-up. These results suggest that the individual contribution from wind or wave forcing alone could be greater than the combined contributions for bed profiles with extreme slopes. The variability of wave set-up and the sensitivity of wind-induced set-up to bathymetry leads us to the conclusion that the relative importance of the wave forcing increases over steeper coastal profiles.

4.2 Hindcast

The addition of wave forcing improves our overall predictive capabilities and can reduce the RMS error by 20% to 50% depending on location. From the contour plots we see that the wave set-up acts to offset the blow-down and amplify the set-up generated by the wind and pressure. The effect of waves on surge is also evident before the storm makes landfall since the waves reach the shore several hours before the peak winds. Set-up is most

prominent in the bays and coastal lakes. The model predicts that waves alone can account for more than one meter of surge, as is the case in Perdido Bay where the wave set-up was more than half the total surge predicted with the combined forcing. Over the whole domain the maximum surge from the waves amounted to more than 30% of the maximum water level predicted in the domain. During the peak of the storm event, the prediction and the recorded water levels are in close agreement when we include the wind, pressure and wave forcing. The addition of waves can allow for as much as a 60% increase in predictive power as shown by the analysis at Pensacola Bay.

4.3 Significance of Wave Set-Up

Waves and wave momentum flux are an important part of the natural system responsible for storm surge. The significance of the wave set-up, and therefore the inclusion of wave forcing in model predictions, is dependent on the bathymetric profile in the path of the storm. If there is a wide, shallow shelf, there will be greater wind set-up at the shoreline. When wind-induced set-up dominates, the waves are not as significant. The wave forces, however, remain an active participant in generating storm surge at different phases of storm passage and in regions farther away from the location of the eye of the storm, and should be kept in the computational models for completeness.

Waves can account for more than one meter of set-up for our predictions of hurricane Georges. In general we have found that waves provide on the order of one-third of the set-up along the coast during hurricane Georges. The wave forcing is an important factor in our case for improving the modeled response of hurricane storm surge.

5 Acknowledgments

Our work is a component of a real-time wind, wave, and surge forecasting system for tropical cyclones being developed under the National Oceanographic Partnership Program (NOPP). This partnership involves four academic institutions and six government agencies, sharing data, models, and resources. Wind, wave, and barometric pressure data was provided within the domain by our NOPP partners. Data providers include Scott Hagen at the University of Central Florida, Vince Cardone and Andrew Cox at OceanWeather, Inc., and Robert Jensen at US Army Corps of Engineers. The NOPP is funded by the US Office of Naval Research, Grant # N00014-02-1-0150. The finite element grid was provided by Rick Luettich of the University of North Carolina.

References

R. A. Anthes. *Tropical Cyclones, Their Evolution Structure and Effects*. American Meterological Society, Boston, Mass., 1982.

C. A. Blain. Modeling methodologies for the prediction of hurricane storm surge. *Recent Advances In Marine Science and Technology*, 96:177–189, 1997.

C. A. Blain, J. J. Westerink, and R. A. Luettich. The influence of domain size on the response characteristics of a hurricane storm surge model. *Journal of Geophysical Research*, 99:18,467–18,479, 1994.

C. A. Blain, J. J. Westerink, and R. A. Luettich. Grid convergence studies for the prediction of hurricane storm surge. *International Journal for Numerical Methods in Fluids*, 26:369–401, 1998.

C. A. Brebbia, L. Traversoni, and L. C. Wrobel, editors. Application of a Domain Size and Gridding Strategy for the Prediction of Hurricane Storm Surge. In: *Computer Modelling of Seas and Coastal Regions II*, pages 301–308. Computational Mechanics Publications, Southampton, UK, 1995.

R. G. Dean and R. A. Dalrymple. *Water Wave Mechanics for Engineers and Scientists*. World Scientific Press, River Edge, New Jersey, 1991.

R. G. Dean and R. A. Dalrymple. *Coastal Processes with Engineering Applications*. Cambridge University Press, Cambridge, UK, 2002.

M. A. Donelan. Air-water exchange processes. *Coastal and Estuarine Studies*, 54:19–36, 1998.

M. A. Donelan, F. W. Dobson, S. D. Smith, and R. J. Anderson. On the dependence of sea surface roughness on wave development. *Journal of Physical Oceanography*, 23:2143–2149, 1993.

J. R. Garratt. Review of drag coefficients over oceans and continents. *Monthly Weather Review*, 105:915–929, 1977.

G. L. Geernaert and W. J. Plant, editors. Bulk Parameterizations for the Wind Stress and Heat Fluxes. In: *Surface Waves and Fluxes I*, chapter 5, pages 91–172. Kluwer Academic Publishers, Netherlands, 1990.

J. L. Guiney. Preliminary report, hurricane georges, 15 september - 01 october 1998. Technical report, NOAA, National Hurricane Center, Miami, Florida, 1999. URL `http://www.nhc.noaa.gov/1998georges.html`. 08/2002.

S. C. Hagen, J. J. Westerink, and R. L. Kolar. One-dimensional finite element grids on a localized truncation error analysis. *International Journal for Numerical Methods in Fluids*, 32:241–261, 2000.

S. C. Hagen, J. J. Westerink, R. L. Kolar, and O. Horstmann. Two-dimensional, unstructured mesh generation for tidal models. *International Journal for Numerical Methods in Fluids*, 35:669–686, 2001.

L. H. Holthuijsen. *SWAN Cycle III version 40.11 User Manual (Not the Short Version)*. Delft University, NL, 2000.

I. D. James. Non-linear waves in the nearshore region: Shoaling and set-up. *Estuarine and Coastal Marine Science*, 2:207–234, 1974.

P. D. Komar. *Beach Processes and Sedimentation*. Prentice-Hall, Upper Saddle River, New Jersey, 2nd edition, 1998.

G. J. Komen, L. Cavaleri, M. Donelan, K. Hasselmann, S. Hasselmann, and P.A.E.M. Janssen. *Dynamics and Modelling of Ocean Waves*. Cambridge University Press, Cambridge, UK, 1996.

M. S. Longuett-Higgins. Wave set-up, percolation and undertow in the surf zone. *Proceedings of the Royal Scociety of London, Series A, Mathematical and Physical Sciences*, 390:283–291, 1983.

M. S. Longuett-Higgins and R. W. Stewart. Radiation stresses in water waves; a physical discussion with applications. *Deep-Sea Research*, 11: 529–562, 1964.

R. A. Luettich, J. J. Westerink, and N. W. Sheffner. Adcirc: An advanced three-dimensional circulation model for shelves, coasts and estuaries. report 1: Theory and methodology of adcirc-2ddi and adcirc-3dl with applications. Technical Report DRP-92-6, Department of the Army, Washington, DC, 1992.

W. G. McDougal and R. T. Hudspeth. Non-planar beaches: Wave induced setup/setdown and longshore current. Technical Report ORESU-R-81-016, Oregon State University Sea Grant College Program, Corvalis, Oregon, 1981.

T. Saville. Experimental determination of wave set-up. *National Hurricane Research Project Report*, 50:242–252, 1961.

M. J. F. Stive and H. G. Wind. A study of radiation stress and set-up in the nearshore region. *Coastal Engineering*, 6:1–25, 1982.

P. J. Turner and A. M. Baptista. *ACE/gredit Online Documentation.* Oregon Health & Science University, Center for Coastal and Land-Margin Research (CCALMR), Beaverton, Oregon, 1999. URL `http://www.ccalmr.ogi.edu/software/xmgredit5/`. 11/2002.

List of Figures

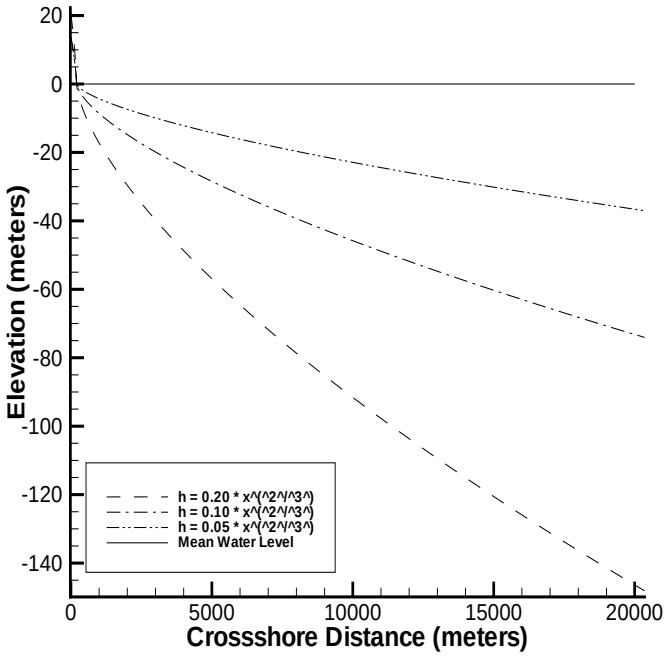

Figure 1: Bathymetric contours created to test the wave and wind set-up

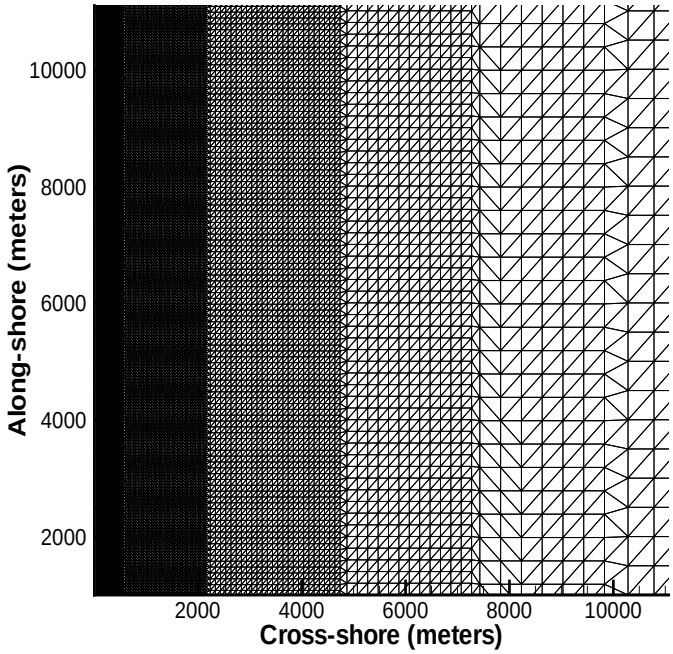

Figure 2: Finite Element Grid created with ACE/gredit (resolution at the shoreline is 20 m)

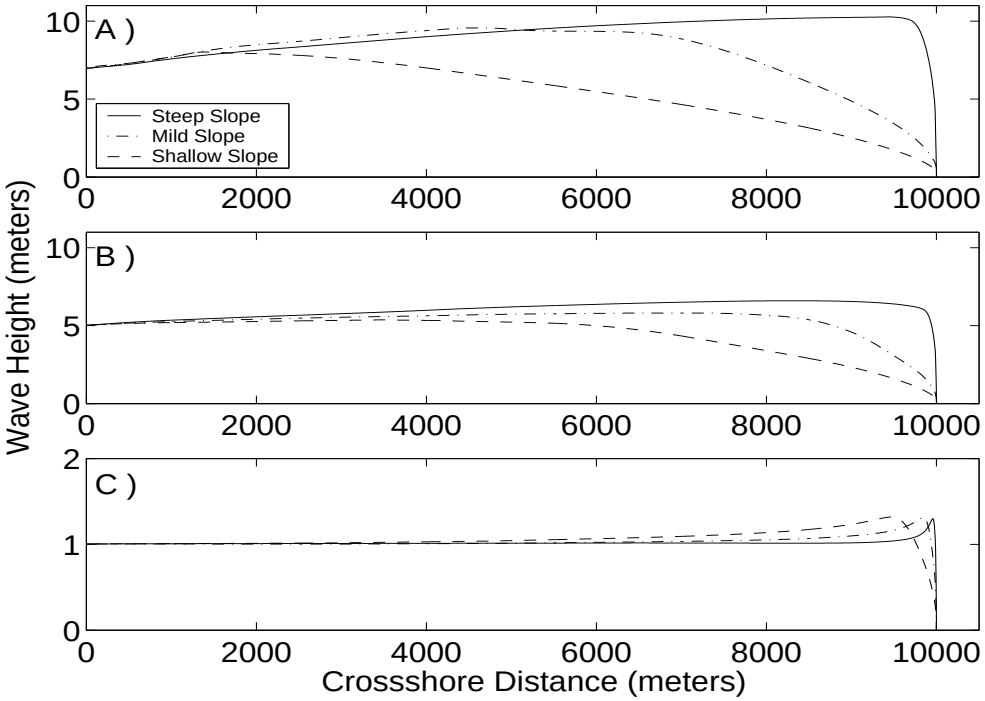

Figure 3: The wave fields output by SWAN over the three bathymetric contours. A) Strong forcing. B) Medium forcing. C) Weak forcing.

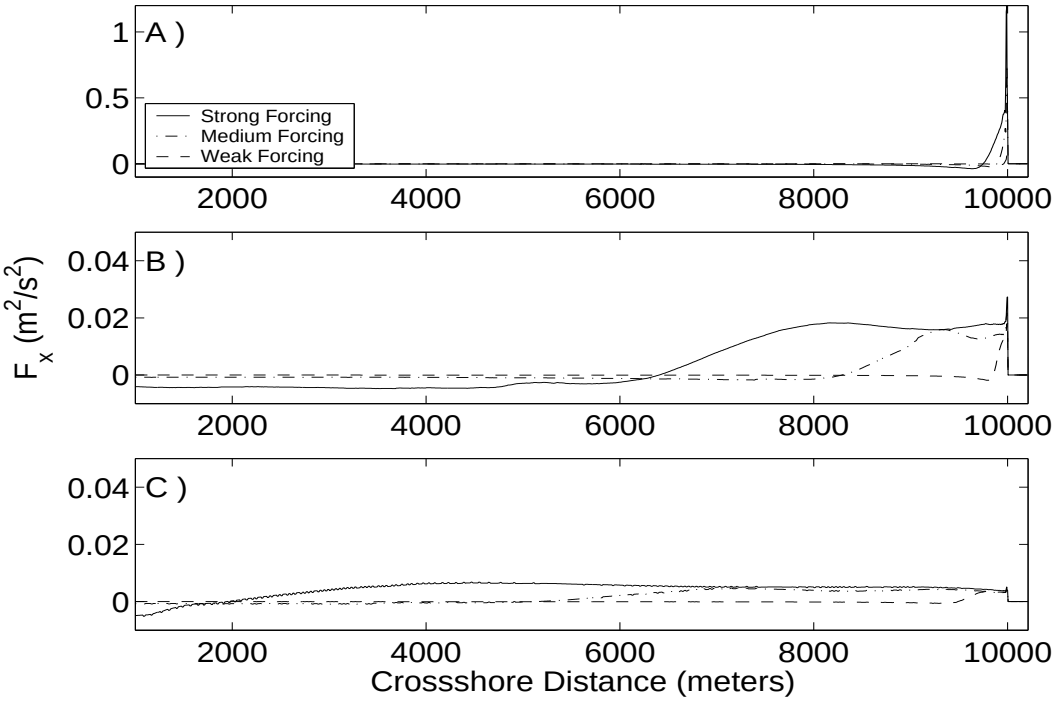

Figure 4: The F_x output field from SWAN for each of the three forcing strengths (the value of the forcing is given by Equation 17). A) Steep slope. B) Mild slope. C) Shallow slope.

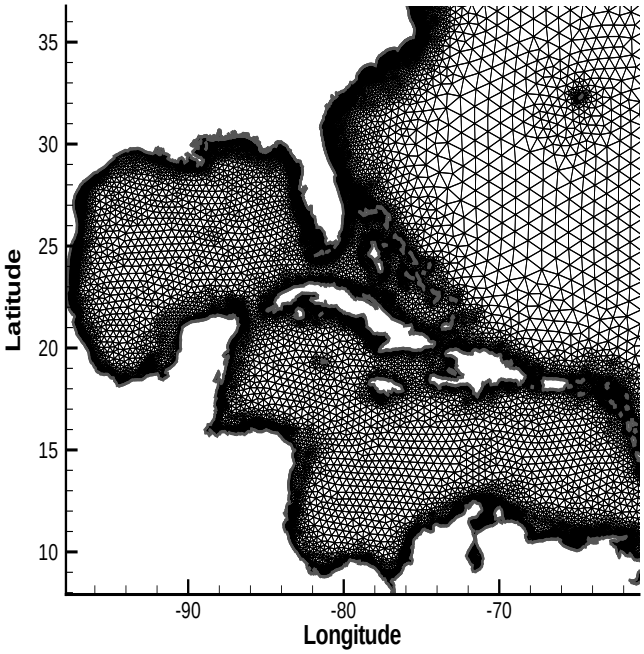

Figure 5: Finite Element Grid of the Northwest Atlantic Domain consisting of 31435 Nodes and 58369 Elements. The nodal spacing is 0.03 to 0.06 degree at the coast, 0.016 degree in the inlets, and about 0.5 deg maximum spacing in the Gulf of Mexico.

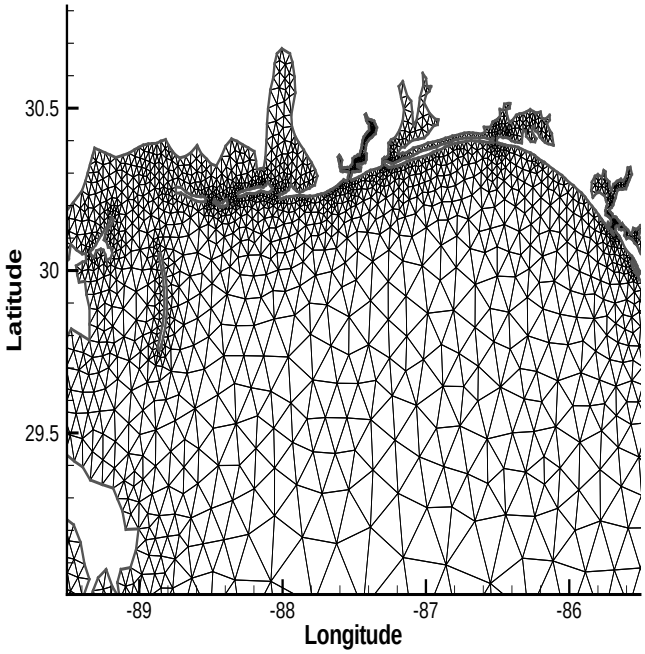

Figure 6: The Gulf Coast region of our model domain (Louisiana to Florida). This is where hurricane Georges made landfall in the Continental U.S.

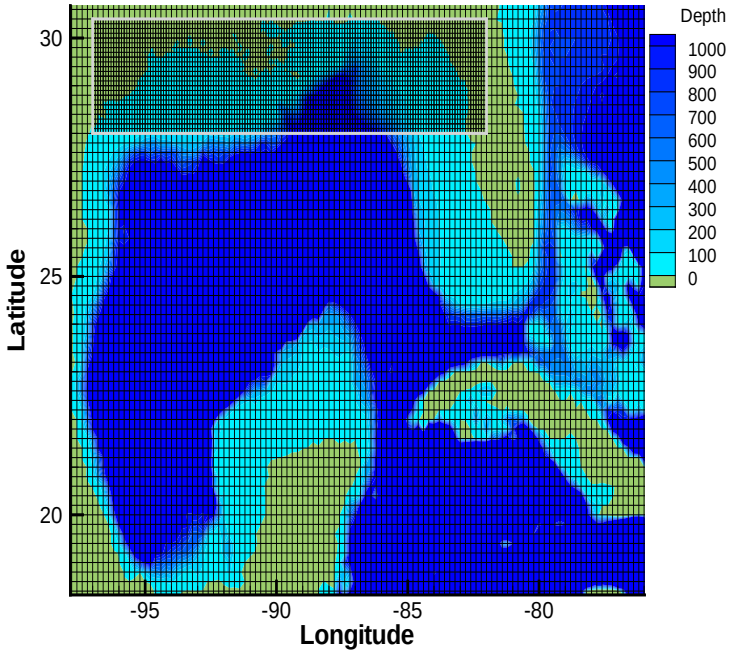

Figure 7: The wave fields are provided at two levels of resolution. Near the region of landfall the waves are given at every 0.1 degree. In the Gulf of Mexico basin the waves are given at every 0.2 degree.

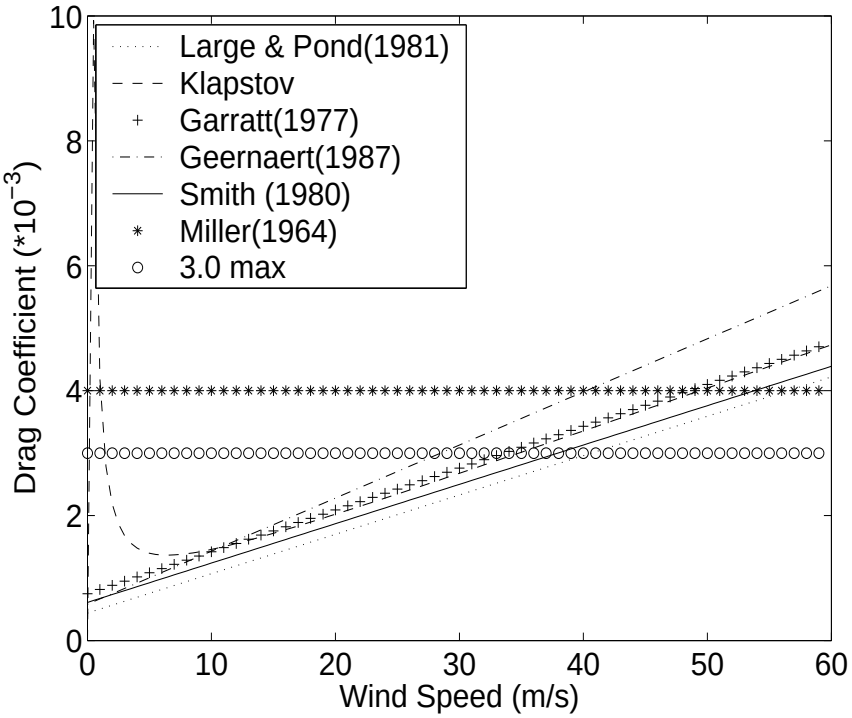

Figure 8: The seven drag coefficient formulations plotted vs. wind speed.

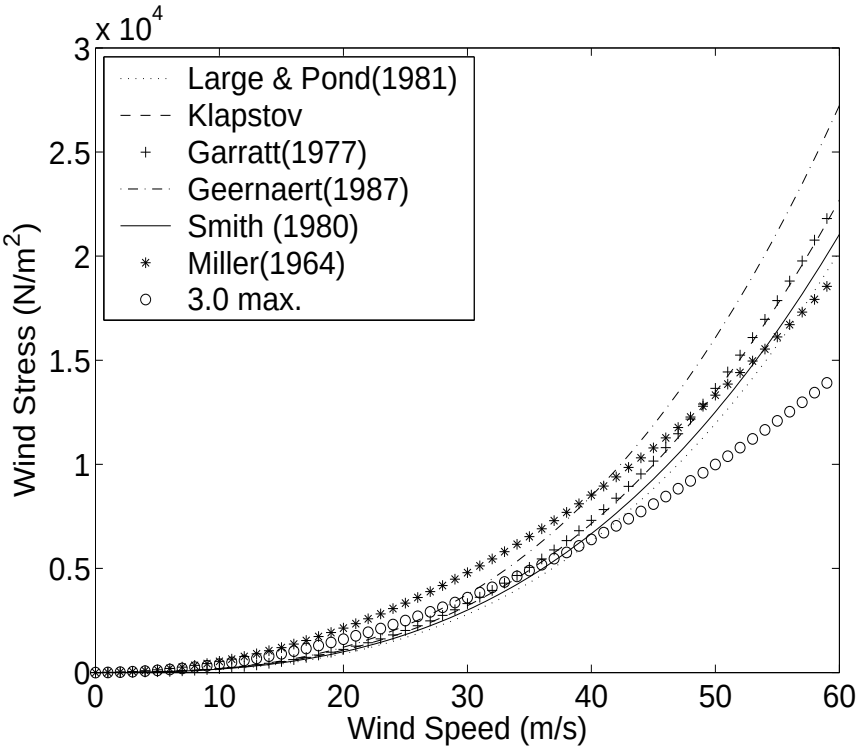

Figure 9: Wind stress calculated using the different drag formulas and the cutoff value, plotted vs. wind speed.

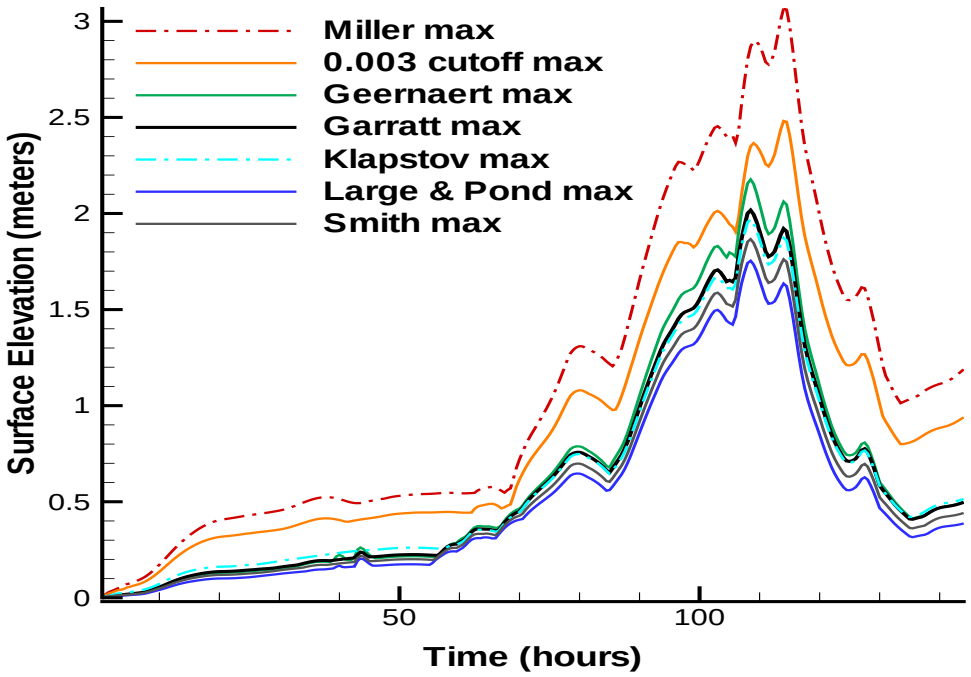

Figure 10: Maximum and minimum surge generated for each of the wind stress formulations using the seven different drag coefficients.

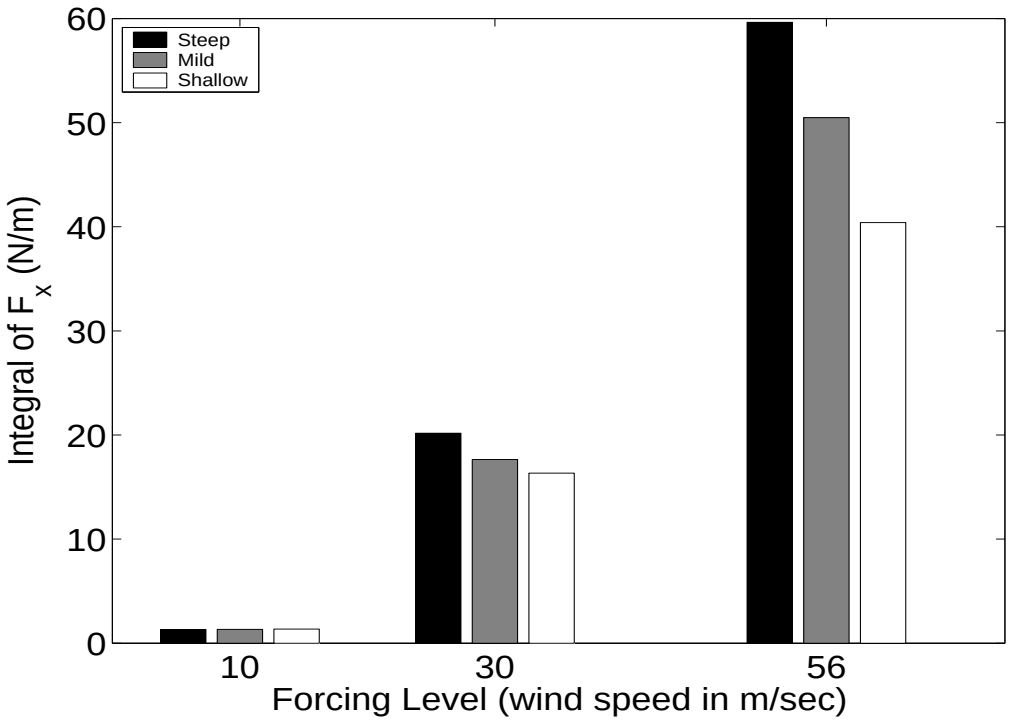

Figure 11: The integral sum of $\overline{F}$ output by SWAN for the three different forcings over the three bathymetric profiles. The value of the forcing is given by Equation 17

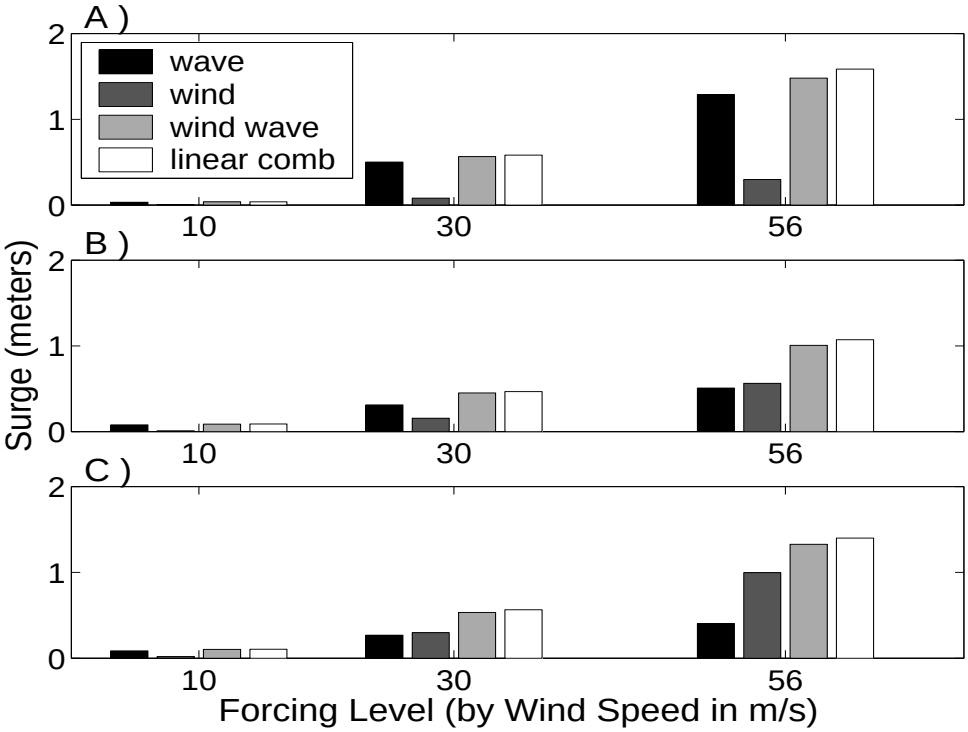

Figure 12: The surge levels for each forcing group over each bottom topography (data from Table 4) A) Steep slope. B) Mild slope. C) Shallow slope. The wind-wave entry represents the combined forcing for the model run. The linear combination entry represents the sum of the surge predicted from the wind forcing, and that predicted using only the wave forcing.

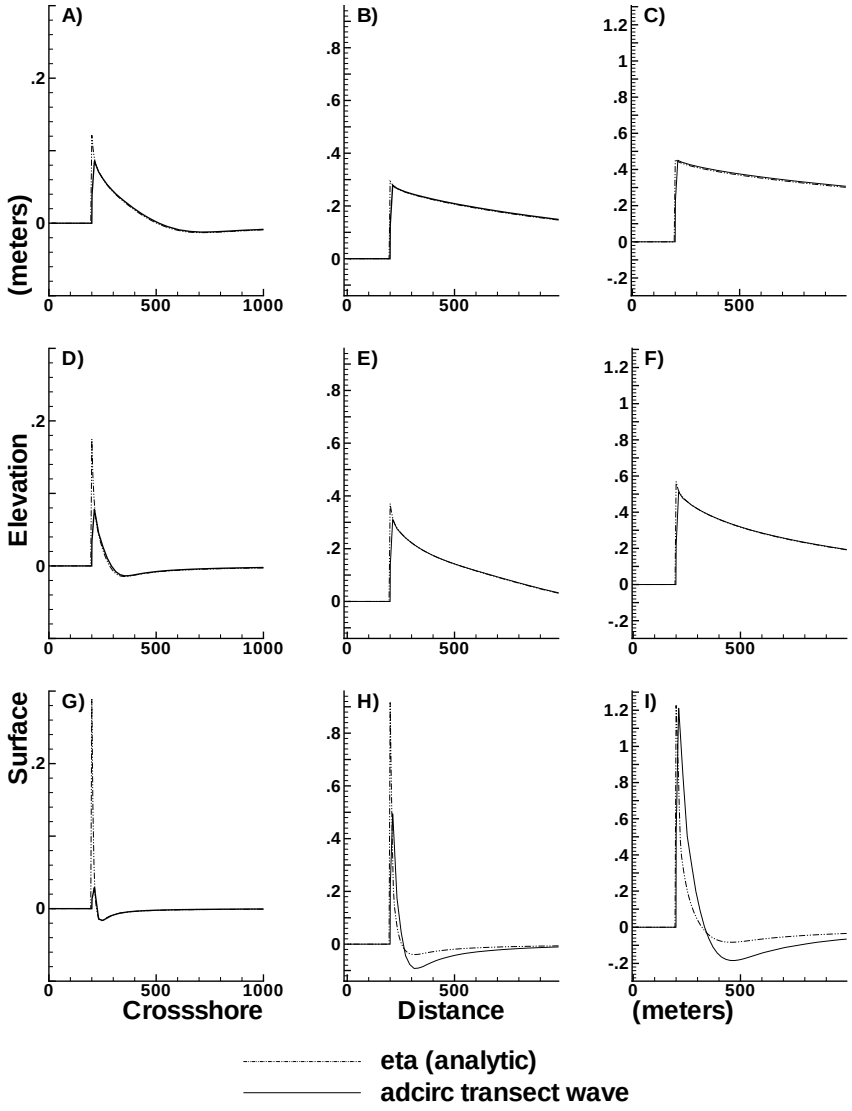

Figure 13: Comparison of Model results for wave forcing with the analytic solution for steady state wave set-up. Shown are all nine profile and forcing combinations (note the change in scale along the y-axis as the forcing increases): A) Shallow profile, weak forcing. B) Shallow profile, medium forcing. C) Shallow profile, strong forcing. D) Mild profile, weak forcing. E) Mild profile, medium forcing. F) Mild profile, strong forcing. G) Steep profile, weak forcing. H) Steep profile, medium forcing. I) Steep profile, strong forcing.

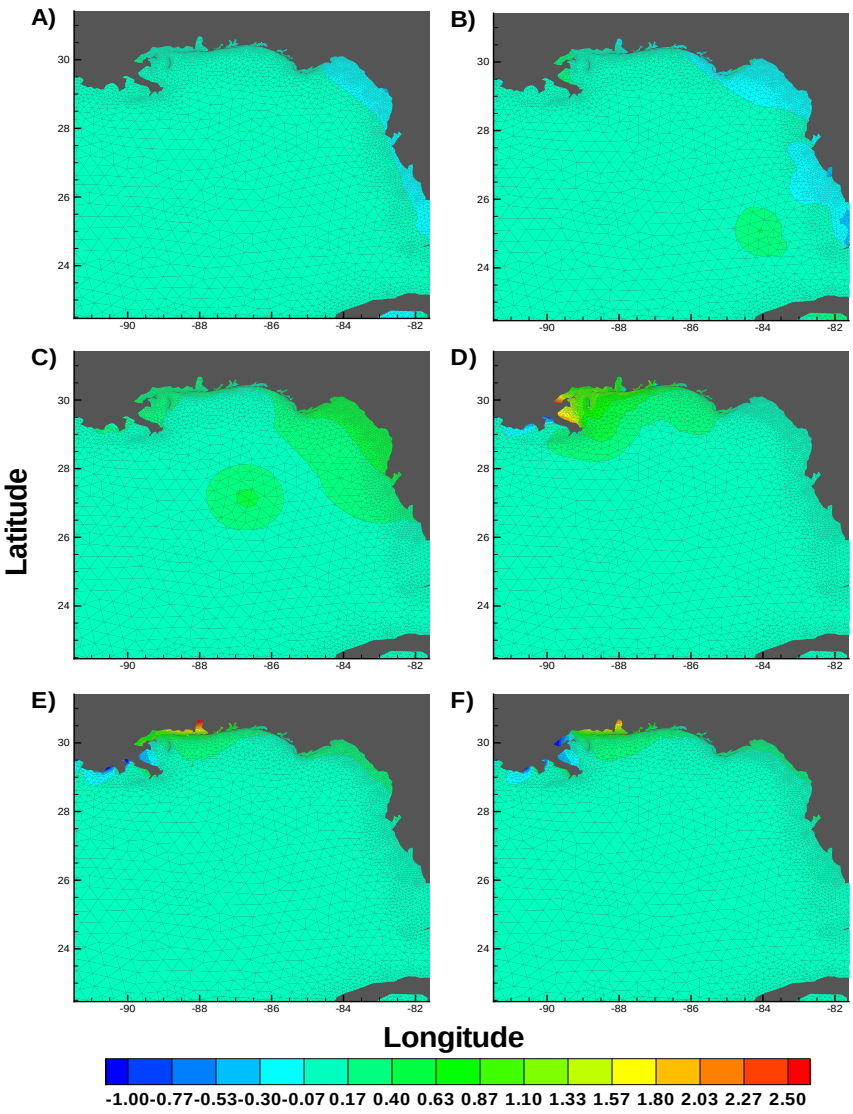

Figure 14: A series of surface contour plots shows the surge as hurricane Georges makes its way across the Gulf of Mexico and makes landfall (prediction was made with the combined forcings). A) t = 10 hours into the simulation. B) t = 30 hours. C) t = 50 hours. D) t = 70 hours. E) t = 90 hours. F) t = 110 hours.

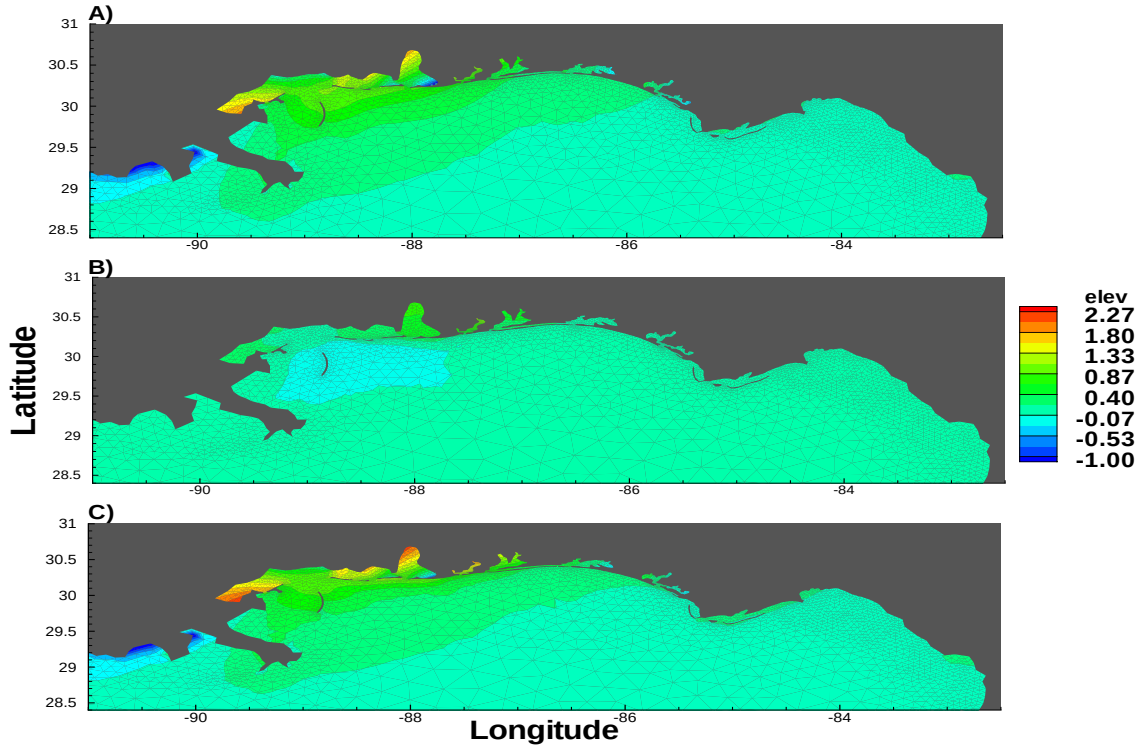

Figure 15: A series of surface contour plots shows the surge as hurricane Georges make landfall, t=82 h. A) Surface elevation generated from the meteorological forcing. B) Surge created by wave forcing. C) Surge generated from the combined forcing.

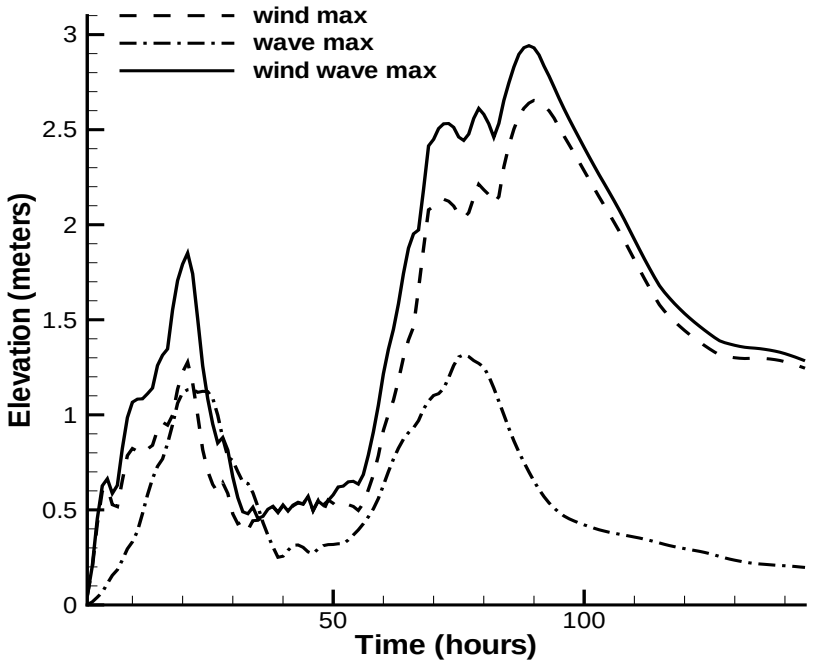

Figure 16: For each set of model prediction forcings, the maximum water surface elevation is plotted at every time step.

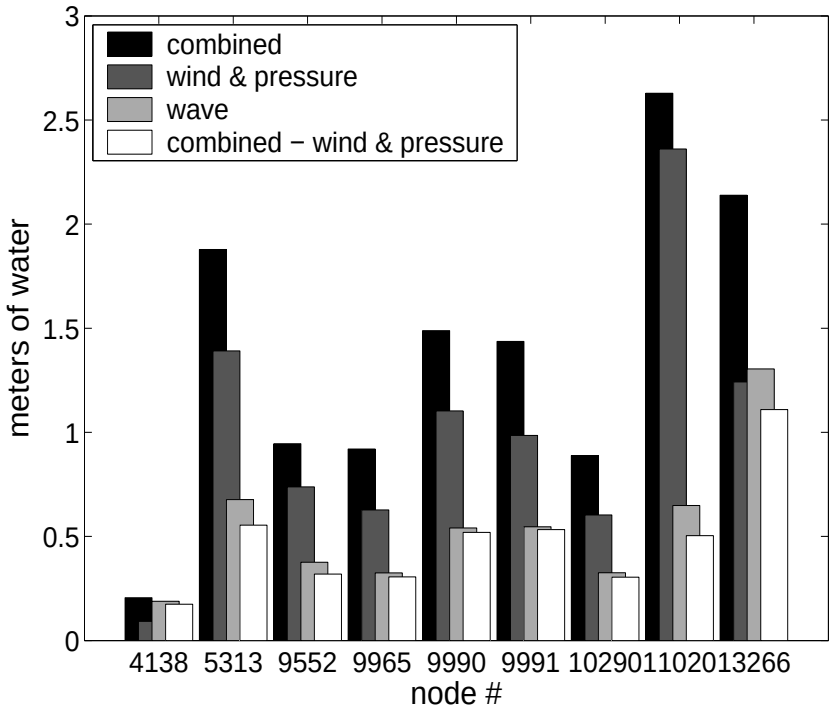

Figure 17: For the specified nodes given in Table 5, we plot the maximum surge over the duration of the simulation for combination of each forcing. Also plotted is the maximum difference between the combined forcing and wind only forced elevation.

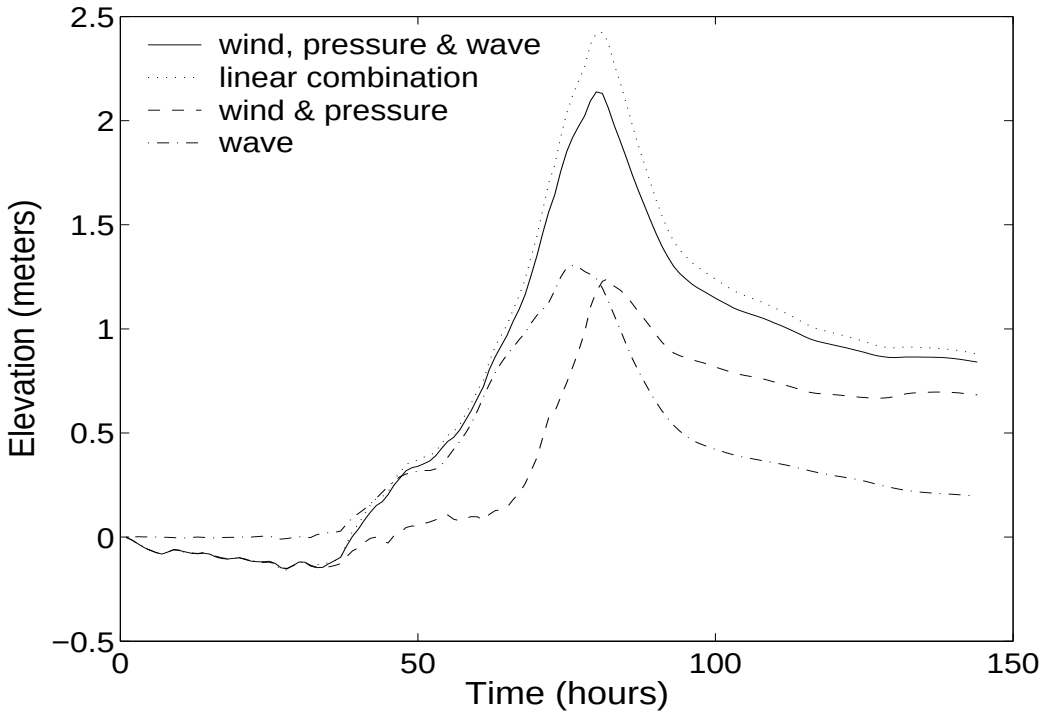

Figure 18: The water level at Node–13266:Perdido Bay, FL. We show the surge as predicted by the meteorological forcing, the wave forcing, and the combined forcing. Also plotted is the linear combination of the two individually forced model results.

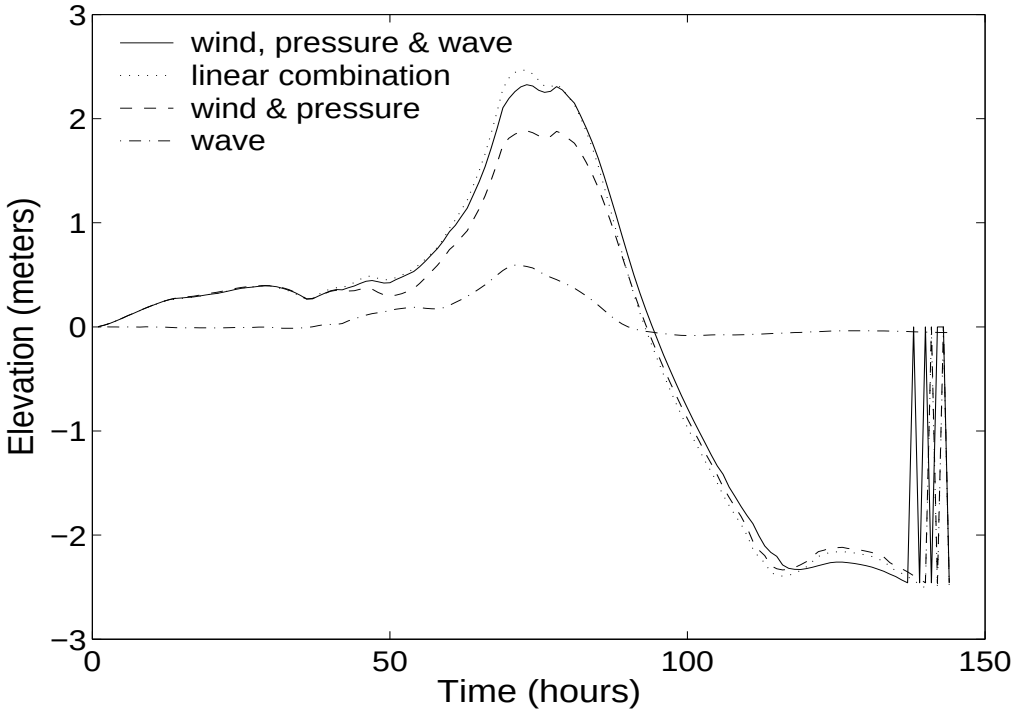

Figure 19: The water level at Node–11043:Lake Borgne, LA. We show the surge as predicted by the meteorological forcing, the wave forcing, and the combined forcing. Also plotted is the linear combination of the two individually forced model results.

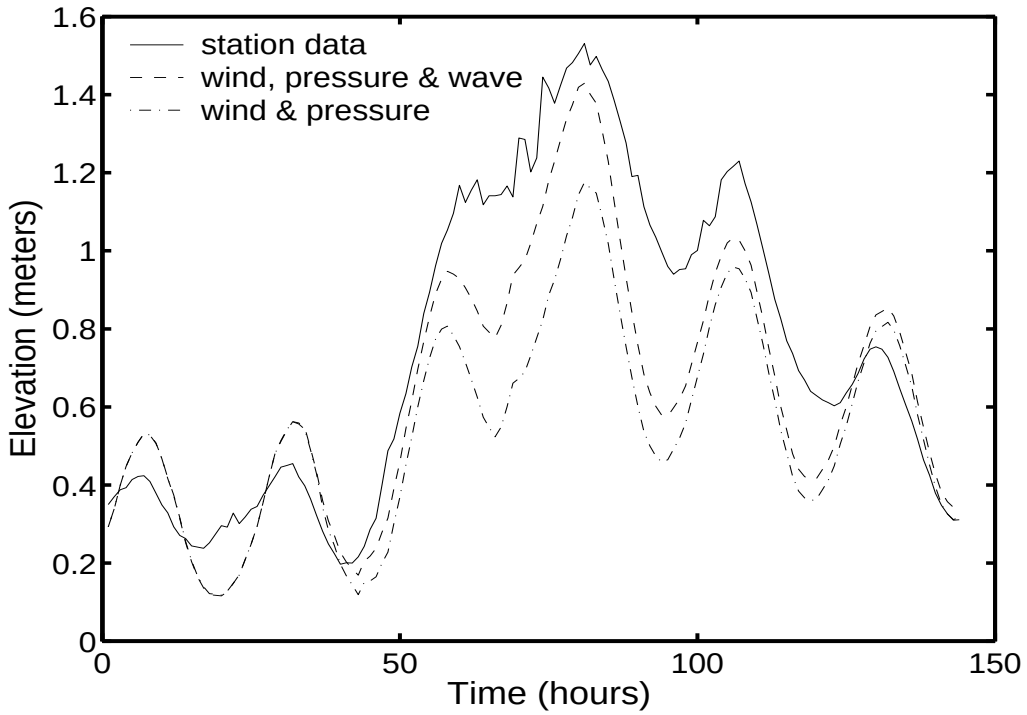

Figure 20: Forced by the combination of wave and meteorological inputs, the output from the ADCIRC model at Pensacola Bay is plotted with the historical data recorded by the station at the same corresponding time period. Our prediction is translated in order to more closely match the start time mean water level at the station.

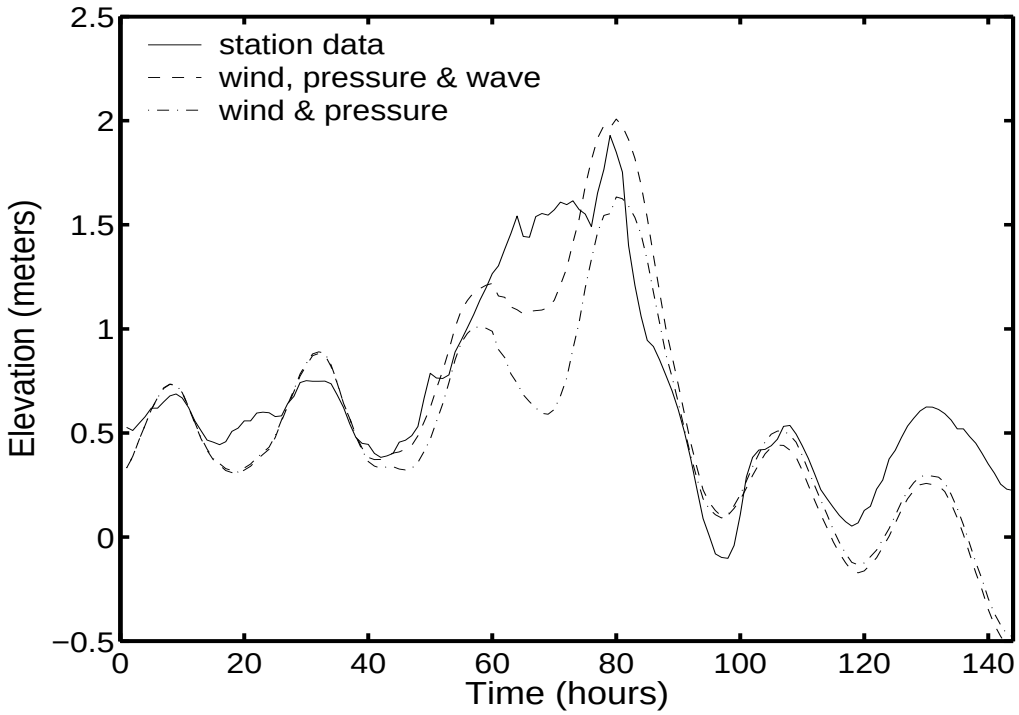

Figure 21: Forced by the combination of wave and meteorological inputs, the output from the ADCIRC model at Waveland is plotted with the historical data recorded by the station at the same corresponding time period. Our prediction is translated in order to more closely match the start time mean water level at the station.

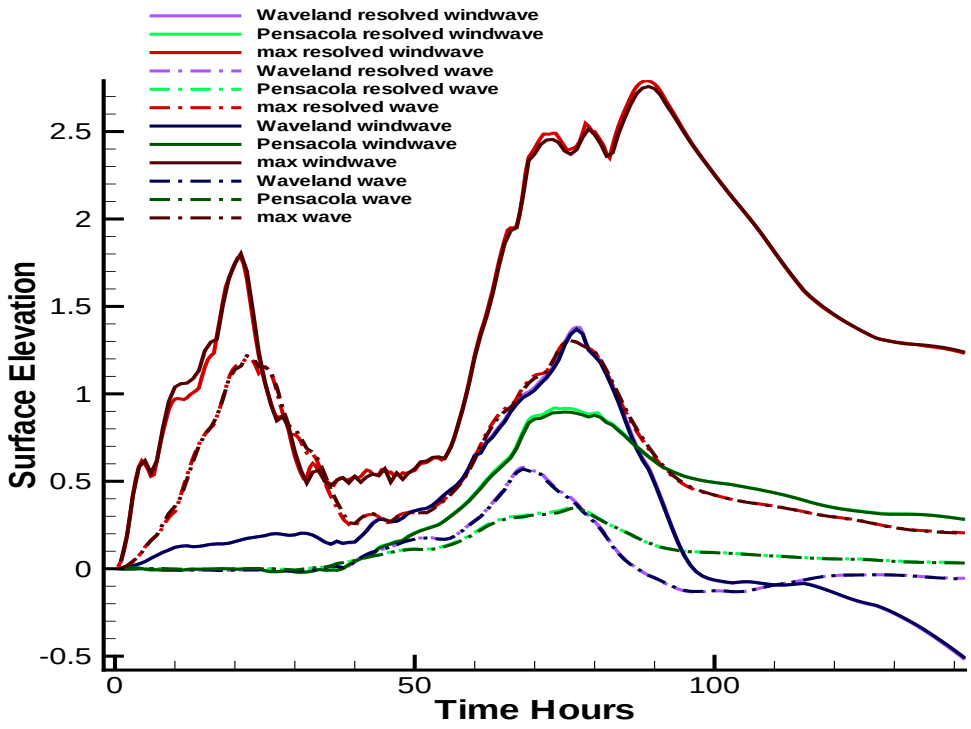

Figure 22: We compare the surface response to combined forcing and wave only forcing at the Pensacola location and the Waveland location. Also plotted is the maximum surface elevation over the whole domain for the two forcing combinations. For the resolved case, the finite element grid has 121296 nodes, compared to the 31435 nodes of the current grid.

List of Tables

Table 1: Drag coefficient formulations used to test model sensitivity

Authors	$C_d * 10^3$
Garratt (1977)	$0.75 + 0.067\|U\|$
Miller (1964)	4.0
Klapstov (1983)	$0.49 + 0.07\|U\| + \frac{2.58}{\|U\|} - 1.06\frac{(T_{air}-T_{sfc})}{\|U\|^2}$
Geernaert (1987)	$0.58 + 0.085\|U\|$
Smith (1980)	$0.61 + 0.063\|U\|$
Large & Pond (1981)	$0.44 + 0.063\|U\|$

Table 2: Wind intensity and off-shore wave height used to force the circulation model for the bathymetry tests

Strength	Wind(m/s)	Wave(m)
Weak	10	1.0
Medium	30	5.0
Strong	56	7.0

Table 3: Model and forcing domains

Domain	S-N	W-E
NW Atlantic FE Grid	8N-46N	98W-60W
Wind and Pressure	5N-53N	99W-50W
Wave Basin	18N-31N	98W-75W
Wave Region	28N-30.4N	97W-82W

Table 4: Maximum calculated surge for forcing components over each bathymetric profile

Bathy	Strength	Wave(m)	Wind(m)	Wind&Wave(m)	Linear Combination(m)
Shallow	Weak	0.079	0.02	0.10	0.10
Shallow	Medium	0.27	0.30	0.53	0.56
Shallow	Strong	0.40	1.00	1.33	1.40
Mild	Weak	0.085	0.01	0.09	0.09
Mild	Medium	0.31	0.16	0.45	0.47
Mild	Strong	0.51	0.56	1.00	1.07
Steep	Weak	0.032	0.005	0.037	0.037
Steep	Medium	0.50	0.08	0.56	0.58
Steep	Strong	1.29	0.30	1.48	1.59

Table 5: Locations of selected tidal stations

Node	Latitude	Longitude	Location
4138	29.2915	-89.9288	Grande Isle, LA
5313	29.3551	-89.3419	Grande Pass, LA
9552	30.2546	-88.1925	Dauphin Island, AL
9965	30.3807	-87.2435	Pensacola, FL
9990	30.2086	-89.3807	Waveland, MS
9991	30.2452	-89.4003	Waveland, MS
10290	30.3888	-87.2261	Pensacola, FL
11020	30.6678	-87.9489	Mobile Bay, AL
11043	29.9664	-89.7226	Lake Borgne, LA
13266	30.4823	-87.4180	Perdido Bay, FL